Modeling the Impact of Biopores on Root Growth and Root Water Uptake

Article *in* Vadose Zone Journal · March 2019

DOI: 10.2136/vzj2018.11.0196

9 authors, including:

Magdalena Landl
Forschungszentrum Jülich
7 PUBLICATIONS 39 CITATIONS
SEE PROFILE

Andrea Schnepf
Forschungszentrum Jülich
80 PUBLICATIONS 1,320 CITATIONS
SEE PROFILE

Daniel Uteau
Universität Kassel
49 PUBLICATIONS 382 CITATIONS
SEE PROFILE

Stephan Peth
Universität Kassel
152 PUBLICATIONS 2,486 CITATIONS
SEE PROFILE

Published March 28, 2019

Original Research

Core Ideas

- A 3D soil–root model was used to investigate root–biopore interactions.
- Known effects of biopores on root growth, i.e., increased root length and depth were reproduced.
- Despite reducing root–soil contact, biopores led to increased water uptake in dry periods.
- Biopores had a larger impact on water uptake for more compact and less conductive soils.

Modeling the Impact of Biopores on Root Growth and Root Water Uptake

Magdalena Landl,* Andrea Schnepf, Daniel Uteau, Stephan Peth, Miriam Athmann, Timo Kautz, Ute Perkons, Harry Vereecken, and Jan Vanderborght

Roots are known to use biopores as preferential growth pathways to overcome hard soil layers and access subsoil water resources. This study evaluates root–biopore interactions at the root-system scale under different soil physical and environmental conditions using a mechanistic simulation model and extensive experimental field data. In a field experiment, spring wheat (*Triticum aestivum* L.) was grown on silt loam with a large biopore density. X-ray computed tomography scans of soil columns from the field site were used to provide a realistic biopore network as input for the three-dimensional numerical R-SWMS model, which was then applied to simulate root architecture as well as water flow in the root–biopore–soil continuum. The model was calibrated against observed root length densities in both the bulk soil and biopores by optimizing root growth model input parameters. By implementing known interactions between root growth and soil penetration resistance into our model, we could simulate root systems whose response to biopores in the soil corresponded well to experimental observations described in the literature, such as increased total root length and increased rooting depth. For all considered soil physical (soil texture and bulk density) and environmental conditions (years of varying dryness), we found biopores to substantially mitigate transpiration deficits in times of drought by allowing roots to take up water from wetter and deeper soil layers. This was even the case when assuming reduced root water uptake in biopores due to limited root–soil contact. The beneficial impact of biopores on root water uptake was larger for more compact and less conductive soils.

Abbreviations: CT, computed tomography; DAS, days after sowing; HC, hydraulic conductivity; LAI, leaf area index; RLD, root length density; SWP, soil water potential.

M. Landl, A. Schnepf, H. Vereecken, and J. Vanderborght, Forschungszentrum Jülich GmbH, Agrosphere (IBG-3), 52425 Jülich, Germany; D. Uteau and S. Peth, Dep. of Soil Science, Univ. of Kassel, 34125 Kassel, Germany; M. Athmann and U. Perkons, Institute of Crop Science and Resource Conservation, Dep. of Agroecology and Organic Farming, Univ. of Bonn, 53121 Bonn, Germany; T. Kautz, Albrecht Daniel Thaer-Institute of Agricultural and Horticultural Sciences, Humboldt Univ. of Berlin, 10099 Berlin, Germany. *Corresponding author (m.landl@fz-juelich.de).

Received 1 Nov. 2018.
Accepted 11 Jan. 2019.
Supplemental material online.

Citation: Landl, M., A. Schnepf, D. Uteau, S. Peth, M. Athmann, T. Kautz, U. Perkons, H. Vereecken, and J. Vanderborght. 2019. Modeling the impact of biopores on root growth and root water uptake. Vadose Zone J. 18:180196. doi:10.2136/vzj2018.11.0196

The ability of plants to extract water from the soil is referred to as *plant water accessibility* and is determined by the architecture of the root system as well as by various interaction processes in the soil–plant continuum (Colombi et al., 2018). One of the most important constraints limiting plant water accessibility is soil penetration resistance with its direct impact on root elongation (Bengough et al., 2011). Soil penetration resistance is positively correlated with soil bulk density and the absolute value of the soil matric potential (Gao et al., 2012; Whalley et al., 2007). Higher soil penetration resistance leads to lower root growth rates and in consequence to less extended root systems with reduced ability to take up water from deeper soil layers (Bengough et al., 2011; Chen et al., 2014; Colombi et al., 2018; Tracy et al., 2012; Valentine et al., 2012). This is an issue in particular during prolonged dry spells when the upper soil layers are water depleted and when the subsoil water supply has high potential value for plant transpiration (Gaiser et al., 2013; Kirkegaard et al., 2007).

An opportunity for roots to overcome compact soil layers and to grow into greater depths is the use of large-sized biopores (diameters >2 mm) as preferential growth pathways (Kautz, 2015; McKenzie et al., 2009; Stirzaker et al., 1996). Biopores are generally vertically oriented, tubular-shaped cavities in the soil formed by decayed plant roots or earthworm burrowing (Kautz, 2015; Naveed et al., 2016). Their abundance depends on soil management and cropping sequence (Han et al., 2015; Kautz et al., 2010), and they can persist for

many years in subsoil horizons below the plow layer (Edwards et al., 1988; Shipitalo et al., 2004). Higher soil compaction was found to increase the amount of roots growing in biopores (Gaiser et al., 2013; Hirth et al., 2005), and these roots were shown to elongate faster and deeper (Hirth et al., 2005; Stirzaker et al., 1996).

The probability of roots remaining within biopores and continuing to grow along them was demonstrated to be higher if biopores were aligned more vertically (Dexter and Hewitt, 1978; Hirth et al., 2005; Stirzaker et al., 1996) and if pore walls were smooth (Hirth et al., 2005; Stirzaker et al., 1996). Large-sized biopores are usually air filled (Fredlund and Xing, 1994), and root water uptake is thus limited to the contact area between root and biopore wall. In a field study, Athmann et al. (2013) observed that 85% of barley (*Hordeum vulgare* L.) and oilseed rape (*Brassica napus* L.) roots found in biopores maintained direct contact with the pore wall. Using analytical solutions, de Willigen et al. (2018) showed that incomplete radial root–soil contact (i.e., a root growing in a preexisting pore with a larger diameter) hardly reduced root water uptake capacity due to compensatory root water uptake, while incomplete axial root–soil contact (i.e., entire axial root parts without soil contact) led to a significant decrease in root water uptake potential.

Direct measurements of the impact of biopores on root growth and root water uptake are difficult. Laboratory experiments (e.g., Hirth et al., 2005; Stirzaker et al., 1996) can give valuable information on the influence of soil structure on both root growth and root water uptake but are limited to young plants, small pot sizes, and short measurement intervals. Field experiments (e.g., Colombi et al., 2017; Kautz et al., 2013; White and Kirkegaard, 2010) provide important insights on the dynamics of root growth in soils with biopores during entire cropping periods but do not allow direct investigation of the influence of soil structure on root water uptake. Simulation models can thereby help to explain the relations among experimental data (e.g., link water use efficiency with soil water content and bioporosity) and to test scenarios of different environmental and soil physical conditions. In recent years, significant progress has been made in the development of crop models, which are used to analyze the performance of cropping systems under variable climate and soil management conditions (Vereecken et al., 2016; Wöhling et al., 2013). These models, however, are usually based on simplifying assumptions such as a uniform root distribution and homogeneous root water uptake in lateral soil horizons. The effect of soil structure is thereby at best taken into account indirectly via stress functions on root elongation (e.g., de Moraes et al., 2018; Gaiser et al., 2013). If the impact of biopores on model input parameters such as root length density development, root system hydraulic conductance, and the relative distribution of root water uptake is known, the effects of structured soil can be taken into account more accurately.

We recently developed a new model approach for the simulation of root growth in structured soil. In this approach, the structure of the biopore network as well as the root architecture are considered in a spatially explicit way and the growth of individual root tips is described as a function of local soil penetration resistance. In test simulations, this model realistically reproduced root growth in artificial macropores on both the single root and the plant root system scales (Landl et al., 2017). Our model approach was incorporated in the three-dimensional numerical R-SWMS (Root–Soil Water Movement and Solute Transport) model (Javaux et al., 2008) and is, to our knowledge, the first explicit three-dimensional simulation model for root architecture development and root water uptake in soil with biopores.

Experimental studies showed that root growth in artificial macropores and naturally created biopores differs significantly. While Stirzaker et al. (1996) found roots to be trapped in straight vertical macropores created with steel rods, Kautz et al. (2013) observed field-grown roots to leave biopores when entering less compact soil layers. An explanation for this discrepancy is the wide range of geometries and orientations covered by naturally created biopores, which contrasts with the generally straight and smooth appearance of artificial pores (Pagenkemper et al., 2013, 2015). For realistic simulations of root growth and root water uptake in structured soil, it is thus necessary to use realistic biopore networks. A possibility to noninvasively reproduce soil structure in three dimensions is X-ray computed tomography (X-ray CT) (Luo et al., 2008; Pagenkemper et al., 2013, 2015; Peth et al., 2008). A simplified reconstruction of the pore space geometry of X-ray CT images can serve as a realistic description of the pore network in simulation models.

In the present study, we evaluated the impact of subsoil biopores on root growth, root water uptake, and root soil exploration using the simulation model R-SWMS. Our model approach for root growth in structured soil was calibrated with extensive experimental field data. A natural biopore system was created using X-ray CT scans of intact soil columns from the field site. We used the calibrated model to simulate scenarios in which we evaluated the impact of subsoil biopores on root growth and root water uptake under different soil physical and environmental conditions. To compute root water uptake, we used the model approach developed by Couvreur et al. (2012), which provides realistic parameters describing root system hydraulic conductance and relative distribution of root water uptake that can directly be used in one-dimensional crop-scale models such as HYDRUS (Cai et al., 2018; Šimůnek et al., 2016).

Materials and Methods

Field Experiment

The model setup was based on a field experiment, which was performed at the study site Klein Altendorf (University of Bonn, Germany, 50°62′ N, 6°98′ E) in 2010. In this experiment, the effect of varying biopore densities on root growth of spring wheat was investigated. The soil at the field site was classified as a Haplic Luvisol (IUSS Working Group WRB, 2014), which is characterized by a silt clay loam texture (4–7% sand, 67–76% silt, 17–29% clay, 2.6–10 g kg^{-1} organic C). Below a plow horizon of

30-cm depth, the soil was well structured, with pronounced biopore networks originating from decayed plant roots as well as from earthworm activity (Kautz et al., 2010, 2014).

After plowing to a depth of 30 cm, spring wheat ('Scirocco') was sown with a density of 400 grains m^{-2} and a row width of 10 cm on 8 Apr. 2010. Root length densities (RLDs) in both the bulk soil and biopores were measured on five occasions with the profile wall method for both alfalfa (*Medicago sativa* L.) and fescue (*Festuca arundinacea* Schreb.) pre-crop treatment (Böhm and Koepke, 1977; Gaiser et al., 2013) (Table 1) down to a soil depth of 80 cm (first four occasions) or 160 cm (last occasion). It is well known that RLDs measured with the profile wall method underestimate actual RLDs (Gaiser et al., 2013). Using the calibration equation established by Gaiser et al. (2013) for this very same field experiment from reference measurements with auger samples, RLDs obtained with the profile wall method were converted to absolute RLDs:

$$RLD = RLD_{pw}\left[3.0092 + 13.5\exp\left(-7.2969\ RLD_{pw}\right)\right] \quad [1]$$

where RLD is the absolute root length density (L L^{-3}) and RLD_{pw} (L L^{-3}) is the root length density measured with the profile wall method.

Leaf area index (LAI), which was needed to partition potential crop evapotranspiration into evaporation and transpiration, was measured with a LI-3100C Area Meter (LI-COR) in 2010 on three occasions between seeding and midseason, as indicated in Table 1. To obtain the entire development of LAI from seeding to harvest, we additionally used measurements from 2012 when a second field trial with identical design adjacent to the first one was also cultivated with spring wheat.

To investigate the biopore system, eight intact soil columns (18-cm o.d., 55-cm height, four from alfalfa and four from fescue pre-crop treatments) were excavated from the subsoil (35–90-cm depth) with a lysimeter driller (UGT GmbH). They were scanned with an industrial X-ray CT scanner (GE phoenix v|tome|x s240, GE Sensing and Inspection Technologies GmbH and processed as described by Pagenkemper et al. (2015). Via segmentation, the obtained gray-scale images were transformed into highly resolved binary image stacks with a resolution of 231 µm displaying only biopore and soil matrix voxels. Using volume thresholding, disconnected pore volumes <0.2 cm^3 were then eliminated to set the focus on the continuous biopore network. The upper parts of all binary image stacks showed unrealistic high bioporosities. This fault, which was also observed in other studies (e.g., Luo et al., 2008; Pagenkemper et al., 2013), is a result of the rotary cutting process used to cut the soil columns from the soil matrix during the excavation process. To obtain realistic biopore networks, we thus eliminated the upper 15 cm of each image stack, thereby reducing the height to 40 cm. Due to the cylindrical shape of the excavated soil columns, the corner regions of the cubic image stacks did not contain biopores. We therefore cropped the outer edges of each image stack in both *x* and *y* directions from 18 to 12 cm.

In general, it is expected that taproot plants such as alfalfa generate large continuous biopore networks, while fibrous root systems such as fescue do not produce large biopores in the subsoil (Pagenkemper et al., 2015). Due to the presence of older biopore systems at our study site, however, differences in biopore networks between the two pre-crop treatments were not as pronounced as could be expected if the preceding crops were planted in homogenized soil (Pagenkemper et al., 2013). The similarity between biopore networks of different origin was also reflected in root length density measurements of spring wheat, where we could not observe large differences between the different pre-crop treatments. A two-sample *t*-test showed that RLD in the bulk soil after fescue pre-crop observed at different times and depths was significantly larger in 9% of all measurements, significantly lower in 35%, and not significantly different in 50% from the RLD in the bulk soil after alfalfa pre-crop. The RLD in biopores was significantly different in only 4% of all measurements after different pre-crop treatments. For modeling purposes, these differences were not sufficiently pronounced. For both biopore network reconstruction and RLD measurement data, we therefore did not distinguish between different pre-crop treatments but used them as replicates.

Modeling Theory

We used the three-dimensional numerical R-SWMS model developed by Javaux et al. (2008) to simulate the impact of biopores on root growth, soil water flow, and root water uptake. The equations and assumptions underlying this mechanistic model as well as the submodels used are presented below.

Simulation of Root System Development

Root system development is explicitly represented in three dimensions using the model approach by Clausnitzer and Hopmans

Table 1. Dates of root length density (RLD) and leaf area index (LAI) measurements of spring wheat in 2010 and 2012, days after sowing (DAS), and, if known, growth stages according to the BBCH scale (Lancashire et al., 1991).

	RLD measurements		LAI measurements			
Measurement no.	Date	DAS/BBCH	Date	DAS/BBCH	Date	DAS
1	31 May–2 June 2010	53–55/33	31 May 2010	53/33	28 May 2012	50
2	14–17 June 2010	67–70/55–58	15 June 2010	68/56	13 June 2012	65
3	28–30 June 2010	81–83/68	30 June 2010	83/68	26 June 2012	78
4	13–16 July 2010	96–99/83			9 July 2012	91
5	27–30 July 2010	110–113/89			30 July 2012	112

(1994). In this approach, the root system is described by a set of user-defined input parameters that determine plant-specific properties such as unimpeded growth speed, branching angles, root trajectory development, and the distance between two successive lateral roots. In addition to these root-system-inherent parameters, environmental impact factors on root system development were considered.

The influence of varying soil strength as well as biopores on root system development is taken into account with the approach by Landl et al. (2017). In this approach, biopores are regarded as an additional soil material with very low penetration resistance. Soil mechanical resistance is expressed by its inverse, soil mechanical conductance, and is handled in analogy to hydraulic conductivity in Darcy's law. Differences in soil strength between the biopore and the soil matrix lead to anisotropic or direction-dependent soil mechanical conductance, which is larger in the direction of the main axis of the biopore and smaller in the radial direction. This anisotropy influences both the direction of root growth and the root growth rate. The orientation of an individual root segment d is computed as

$$d = \mathbf{k}F \quad [2]$$

where $\mathbf{k}$ is the three-dimensional soil mechanical conductance tensor that represents the ease with which a root can penetrate the soil and F is a driving force, which is determined by the orientation of the previous root segment, a random deflection angle, and a tropic component.

It is generally assumed that root elongation E [L T^{-1}] is at its maximum at zero soil penetration resistance and stops completely when a maximum soil penetration resistance R_{max} [P] (where P is used to represent the pressure dimension) is reached (Bengough and Mullins, 1990). We use the empirical equation developed by Veen and Boone (1990) to calculate R_{max} as a function of soil matric potential ψ_m as

$$R_{max} = 4\exp^4 + 2.33\psi_m \quad [3]$$

where R_{max} and ψ_m are expressed in hectopascals. It must be noted that this equation was originally developed for maize (*Zea mays* L.) root growth on sandy loam. However, considering that wheat and maize show similar root growth pressures (Clark et al., 2003) and that the computed values of R_{max} fall well within the range of the measured values of R_{max} specified by Ehlers et al. (1983) for silt loam, we considered this equation valid for our modeling purposes.

Experimental studies on the evolution of root elongation between zero and maximum soil penetration resistance have frequently observed a strong initial decrease followed by a lower reduction rate when approaching maximum soil penetration resistance (Bengough et al., 2011; Bengough and Mullins, 1990; Taylor and Ratliff, 1969). We described this relationship between elongation rate and soil penetration resistance with the inverse of a polynomial relation:

$$E = E_{max}\left[1 - \left(\frac{R}{R_{max}}\right)^{1/2}\right] \quad [4]$$

where E and E_{max} are actual and maximum elongation rates [L T^{-1}] and R and R_{max} are actual and maximum soil penetration resistance [P]. Soil penetration resistance R (hPa) was computed as a function of bulk density ρ_b (g cm^{-3}), soil matric potential ψ_m (hPa) and effective saturation S_e (dimensionless) using the empirical pedotransfer function developed by Whalley et al. (2007):

$$\log_{10}(\ \times 10\ ) = 0.35\log_{10}(|\psi_m \times 10\ |_e) + 0.93\rho_b + 1.26 \quad [5]$$

This pedotransfer function was developed for 12 different, undisturbed soils with diverse matric potentials as well as varying texture, organic C content, and bulk density (1.2–1.65 g cm^{-3}) and can thus be considered valid for a wide range of different soils. It must be noted that soil texture is considered indirectly via effective saturation in this equation.

In addition to soil strength, soil temperature is also considered to limit root elongation. It has been shown that root growth occurs only if the soil temperature lies within a plant- and genotype-specific interval and reaches a maximum at a defined optimum soil temperature (Koevoets et al., 2016; Porter and Gawith, 1999). In our model, reduced root elongation due to sub- or supra-optimal soil temperature is described by a sine-wave-shaped impedance function, which equals zero at the lower (2°C) and upper (25°C) limit and one at the optimum (15°C) soil temperature (Somma et al., 1998). Minimum, maximum, and optimum soil temperature values for spring wheat root growth were derived from Porter and Gawith (1999).

Simulation of Water Flow in the Soil and Root Water Uptake

Water flow in the soil is driven by gradients of soil water potential and described by the Richards' equation (Richards 1931):

$$\frac{\partial\theta}{\partial t} = \nabla(K\nabla\psi) - S \quad [6]$$

where θ is the volumetric water content [L^3 L^{-3}], t is the time [T], K is the unsaturated hydraulic conductivity [L^2 P^{-1} T^{-1}], ψ is the total soil water potential (matric + gravitational) [P] and S is a sink term [L^3 L^{-3} T^{-1}], which is defined positive for root water uptake and negative for root water release.

The relationships between soil water content θ [L^3 L^{-3}], matric potential ψ_m [P]) and hydraulic conductivity K [L^2 P^{-1} T^{-1}] are calculated from soil hydraulic properties via the closed-form expression established by Mualem (1976) and van Genuchten (1980):

$$\theta(\psi) = \theta_r + \frac{\theta_s - \theta_r}{\left[1 + (\alpha|\psi_m|)^n\right]^m} \quad [7]$$

and

$$K(\psi) = K_s \frac{\left\{1 - (\alpha|\psi_m|)^{n-1}\left[1 + (\alpha|\psi_m|)^n\right]^{-m}\right\}^2}{\left[1 + (\alpha|\psi_m|)^n\right]^{m/2}} \quad [8]$$

where θ_r [L^3 L^{-3}] is the residual water content, θ_s [L^3 L^{-3}] is the saturated water content, α is related to the inverse of the air-entry suction [P^{-1}], n and m are shape parameters with $m = 1 - 1/n$, and K_s is the saturated hydraulic conductivity [L T^{-1}].

Due to the large size of our root system (>50,000 root segments), it was computationally infeasible to compute water flow between the soil and root system on the root segment level as proposed by Doussan et al. (1998). We therefore used the implicit approach of Couvreur et al. (2012), where root water uptake is computed at the soil element level, which drastically reduces computation time. In this approach, hydraulic conductances of individual roots are summarized to a single equivalent root system hydraulic conductance, while spatially heterogeneous soil–root interface water potentials are combined to a single equivalent soil water potential (SWP) sensed by the plant. The sink term of an individual soil element is computed as

$$S_k V_k = K_{rs}\left(\psi_{s,eq} - \psi_{col}\right)SSF_k + K_{comp}\left(\psi_{s,k} - \psi_{s,eq}\right)SSF_k \quad [9]$$

where S_k [L^3 L^{-3} T^{-1}] is the sink term in the kth soil element, V_k [L^3] is the volume of the kth soil element, K_{rs} [L^3 P^{-1} T^{-1}] is the equivalent conductance of the root system, $\psi_{s,eq}$ [P] is the equivalent total (matric + gravitational) SWP sensed by the plant, ψ_{col} [P] is the total (matric + gravitational) water potential at the root collar, SSF_k (dimensionless) is the standard sink fraction of the kth soil element, K_{comp} [L^3 P^{-1} T^{-1}] is the compensatory root water uptake conductance, and $\psi_{s,k}$ [P] is the SWP of the kth soil element. While the first term of the equation describes the standard root water uptake under homogeneous SWP distribution, the second term accounts for SWP heterogeneity. The parameters SSF, K_{rs}, and K_{comp} were introduced by Couvreur et al. (2012) as the three macroscopic parameters that describe the hydraulic architecture of a root system: SSF specifies for each soil element the amount of water taken up by the root segments located within this soil element as a fraction of the total plant water uptake under homogeneously distributed SWP, K_{rs} describes the water flow per unit of water potential difference between root collar and soil, and K_{comp} defines the extent of compensatory root water uptake within individual soil elements due to water potential heterogeneity within the soil domain. These macroscopic parameters remain constant for root systems with static architecture and constant hydraulic properties. The parameters SSF and K_{rs} were determined from the numerical solution of the hydraulic tree approach by Doussan et al. (1998), which was run for one single time step. The value of K_{comp} was assumed to equal K_{rs}. This is a valid assumption if root axial hydraulic conductances substantially exceed root radial hydraulic conductances (Couvreur et al., 2012), which is the case for cereal root systems (Meunier et al., 2018).

The equivalent SWP sensed by the plant, $\psi_{s,eq}$, is computed as a function of the distribution of local SWPs as well as standard sink fractions as

$$\psi_{s,eq} = \sum_{k=1}^{M} \psi_{s,k} SSF_k \quad [10]$$

where k is the index of soil elements ranging from 1 to M. For soil elements that do not contain any root segments, SSF_k equals zero. It must be noted that Eq. [9–10] rely on the assumptions that SWP within one soil element is constant and that root radial conductances are much smaller than root axial conductances.

The water potential at the root collar ψ_{col} [P]) is assumed to be equal to the leaf water potential, and the flux at the root collar is set to the actual transpiration rate T_{act} [L^3 T^{-1}]. When no water stress is present, i.e., when the water potential at the collar is above a specified threshold value ψ_{lim}, T_{act} is equal to the potential transpiration rate T_{pot} [L^3 T^{-1}]. Under water stress, T_{act} falls below T_{pot} and is computed as

$$T_{act} = K_{rs}\left(\psi_{s,eq} - \psi_{lim}\right) \quad [11]$$

where ψ_{lim} [P] is the minimal water potential at the root collar, which triggers stomatal closure due to water stress and which was set to the constant value of −15,000 hPa (the permanent wilting point).

Numerical Solution of the R-SWMS Model

For the numerical solution of the water flow equation in R-SWMS, the soil domain is discretized in a regular cubic grid of nodes. Soil hydraulic state variables (e.g., soil water potential and soil water content) as well as parameters that describe local soil properties (e.g., bulk density) are specified explicitly for each soil node. Eight adjacent soil nodes then define one soil element, whose average state variables and parameters are calculated from the nodal values. The root system, which consists of a multitude of straight root segments that are connected with each other, develops within this soil grid. Length and orientation of newly emerging root segments are influenced by the properties of the soil element in which the root tip is located. The resolution of the soil grid is chosen according to the size of the soil domain as well as the length of the simulation period, the required preciseness of the results, and the available computation time. For simulations on the root-system scale, the solution of water flow in the soil is computationally expensive due to large soil domains (>1-m depth) and the long periods that are simulated (up to several months). This makes it necessary to choose a relatively coarse grid resolution (centimeter scale). For simulations of root system development in response to small-scale soil structures such as biopores, however, a finer grid resolution must be used (millimeter scale). We reconciled these opposing needs by introducing two soil grids: a fine soil grid in which biopores were represented and which was used for the simulation of root system development and its architectural response to environmental impact factors and a coarse grid, which was used to compute soil water flow but did not represent biopores. It must be noted that the influence of biopores on soil water flow was therefore neglected. Different soil layers as well as all further soil properties were represented in both grids. Soil water potential distribution, which was computed in the coarse grid, was transferred to the fine grid, where it influenced root system development via its effect on soil penetration resistance.

Coupling Root Growth and Root Water Uptake

Root water uptake is computed using root hydraulic architecture parameters (K_{rs}, K_{comp}, and SSF) that are defined initially for a root system with specific root architecture and root segment hydraulic parameters. If the root system changes, these root hydraulic architecture parameters need to be updated. Root system development is computed dynamically at each time step as a function of local soil properties such as soil penetration resistance, which is a function of soil matric potential (Eq. [5]) and thus also of root water uptake. We took these interdependencies into account by coupling root growth with root water uptake: after specified time intervals, the root growth model was given the updated soil water potential distributions within the soil domain, while root hydraulic architecture parameters were recalculated for the updated root system.

Assumptions in the Simulation of Root Growth and Root Water Uptake in Soil with Biopores

A root segment was considered to be located within a biopore if a minimum of one node of its surrounding grid nodes had biopore properties. Considering that root length units in the profile wall method had an equivalent length of 0.5 cm (Perkons et al., 2014), lateral roots in biopores were only counted if more than 0.5 cm of their length was located within a biopore. We neglected water flow in biopores, which were thus assumed to be air filled at all times. Partial root–soil contact in biopores was assumed to inhibit water flow between soil and root and thus to decrease root radial hydraulic conductivity. Root radial hydraulic conductivity was therefore considered proportional to the part of the root in contact with the bulk soil, i.e., the number of surrounding grid nodes with bulk soil properties. The bulk density of biopore nodes was set equal to zero.

Model Setup

The basic model setup was based on and calibrated with data from the experimental field study i.e., root length densities, soil properties, climate data, and LAI.

Soil Parameterization

We used a rectangular shaped soil domain with dimensions of 3 by 10 by 160 cm. The dimensions in the x and y directions corresponded to interplant and interrow distances, respectively, and the dimension in the z direction to the maximum measured rooting depth (Perkons et al., 2014). The soil domain was discretized into two regular cubic grids of nodes with resolutions of 1 and 0.5 cm for the coarse and fine soil grids, respectively. Our simulated biopores therefore had rather large diameters, >0.5 cm. The soil domain was divided horizontally into five different soil layers (one topsoil layer, a mixing zone between top- and subsoil, and three subsoil layers) whose extents and soil properties were derived from the reference field site profile described by Barej et al. (2014). Using the information on soil texture and bulk density, we estimated soil hydraulic properties by means of the pedotransfer functions developed by Tóth et al. (2015) that were established for continental-scale applications in Europe (Table 2).

From an earlier study by Kautz et al. (2010), we obtained soil penetration resistance measurements that were determined on 10 sampling points at the same field site in Klein-Altendorf on plots grown with sugarbeet (*Beta vulgaris* L.), winter wheat, and winter barley down to a depth of 80 cm with a penetrologger when the soil was at field capacity. In Fig. 1, we compare these measurements with soil penetration resistance values predicted using Eq. [5] for the top four soil layers defined in Table 2. It was not possible to predict the exact measured values; the general evolution of soil penetration resistance with depth, however, could be well reproduced, and we thus considered Eq. [5] to be suitable for our modeling purposes.

Setup of the Biopore Network

The biopore networks used in our simulation study were created with the help of the highly resolved binary image stacks. Before these high-resolution image stacks could be used to set up our simulation biopore network, they had to be upscaled to 0.5 cm, which was the discretization of our fine soil grid. Considering that a significant number of biopores in the original image stacks had diameters smaller than the resolution of our fine soil grid, simple upscaling would have resulted in a strong overestimation of the biopore volume. To satisfy our priority objective of conserving biopore network connectivity while keeping the overestimation of biopore volume at a minimum, we applied the following technique: In a first step, we skeletonized the eight binary image stacks with the

Table 2. Soil properties used in the model setup.

Soil section	Horizon†	Depth	Texture			Bulk density	Soil hydraulic parameters according to van Genuchten (1980)‡				
			Sand	Silt	Clay		θ_r	θ_s	α	n	K_s
		cm	%			g cm^{-3}			hPa^{-1}		cm d^{-1}
Topsoil	Ap	0–30	7	76	17	1.29	0.041	0.4857	0.0103	1.2767	5.08
Mixing zone	E/B	31–40	5	75	20	1.32	0.041	0.4778	0.0056	1.2990	1.56
Subsoil	Bt1	41–75	5	68	27	1.42	0.041	0.4502	0.0047	1.2691	1.31
	Bt2	76–115	4	67	29	1.52	0.041	0.4223	0.0041	1.2468	1.20
	Bw	116–160	6	74	20	1.46	0.041	0.4381	0.0050	1.2732	1.62

† Ap, distinct topsoil disturbed by plowing; E/B, eluviated mineral horizon; Bt, argillic horizon; Bw, weathered B horizon.
‡ θ_r, residual water content; θ_s, saturated water content; α and n, shape parameters; K_s, saturated hydraulic conductivity.

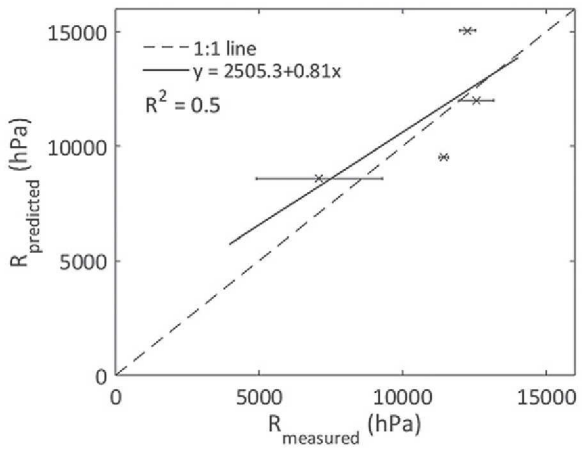

Fig. 1. Measured vs. predicted soil penetration resistance *R* for the individual soil layers of our study site (Table 2) at field capacity. Error bars represent the standard deviation of measurements within one soil layer.

help of the open source software ImageJ, which allowed iterative and symmetric eroding of the biopore surface around its center line. Examples of original and skeletonized images are shown in Fig. 2a and 2b. In a second step, we reduced the resolution of the eight skeletonized images from 231 μm to 0.5 cm (discretization of the simulation domain). If at least one of the original voxels located within the sphere of influence of an upscaled voxel had biopore properties, the upscaled voxel was also assigned biopore properties; an example is given in Fig. 2c. From these eight image stacks, we then cut 12 substacks with 40-cm depth and a cross-sectional area of 3 × 10 cm to obtain images whose size corresponds to the dimensions of our soil domain (example in Fig. 2d). The number of substacks cut from each image stack as well as the location of the cuts was determined with the objective of obtaining clear, continuous biopore networks.

To quantify the modifications of the biopore systems that occurred due to upscaling and image cutting, we determined the pore network parameters bioporosity and biopore length density for the different process steps. Bioporosity [$L^3\ L^{-3}$] is defined as the volume of biopores per volume of bulk soil; biopore length density [$L\ L^{-3}$] is determined as the total length of biopores in a unit soil volume (Luo et al., 2008; Pagenkemper et al., 2013). The upscaling process combined with the assignment of biopore properties to upscaled voxels with at least one original voxel with biopore properties within their vicinity led to an increase in bioporosity from approximately 1.4 to 5% (Image States 1–2; Table 3). Bioporosity then again increased to 10% from the upscaled image stacks to the cut substacks (Image States 2–3; Table 3). This increase, however, was not caused by any image processing but by preserving those parts of the image stacks that contained clear, continuous biopore networks. In contrast to bioporosities, biopore length densities could be kept fairly constant throughout all

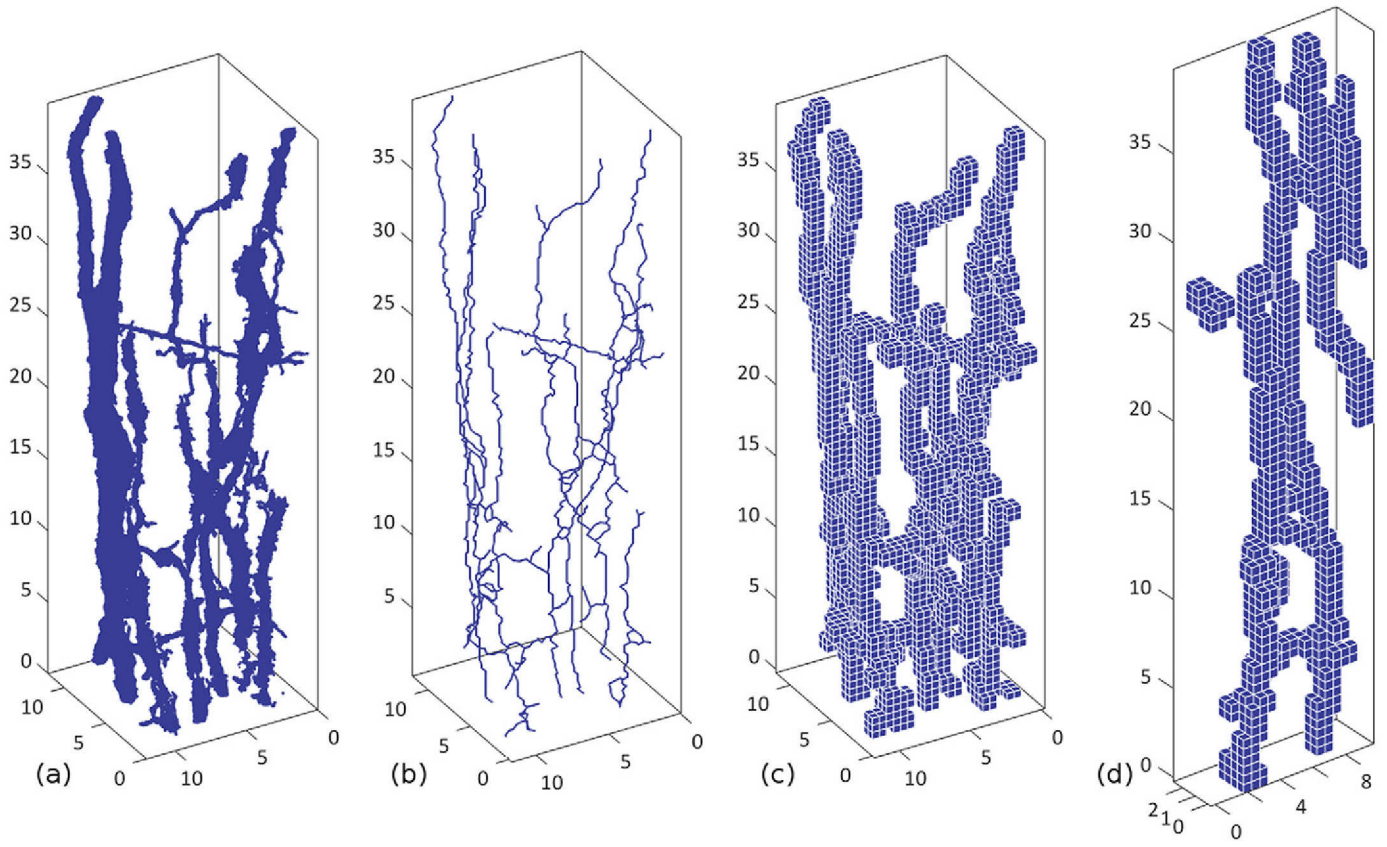

Fig. 2. Examples of (a) binary image stack with a resolution of 231 μm, (b) skeletonized image stack, (c) image stack with a resolution of 0.5 cm, and (d) substack with cross-sectional dimensions of the soil domain.

Table 3. Subsoil bioporosities (bps) and biopore length densities (BPLDs) for images of different processing steps

Image state	Image description	bps	BPLDs
		%	cm cm^{-3}
1	binary image stacks with resolution of 231 μm	1.42 (0.54)†	0.064 (0.016)
2	upscaled image stacks with resolution of 0.5 cm	5.04 (2.05)	0.038 (0.016)
3	substacks with resolution of 0.5 cm cropped to cross-sectional dimensions of soil domain	10.21 (2.76)	0.086 (0.022)

† Mean with standard deviation in parentheses.

process steps. While the upscaling process led to a small decrease in biopore length density from 0.064 to 0.038 cm cm^{-3}, the cropping of the substacks again increased it to 0.086 cm cm^{-3}. These values correspond well to the range of 0.06 to 0.09 cm cm^{-3} that was found by Pagenkemper et al. (2013) for biopore networks of soil monoliths taken from the same field site with the same precrops. It must be noted that the number of biopores remained the same throughout the image processing.

In a last step, we translated the information from the image stacks to three-dimensional coordinate grids by assigning biopore properties to each grid node corresponding to a biopore voxel. Observations from the field experiment showed that root growth in biopores mainly occurred in the subsoil at depths >30 cm. This can be explained by the topsoil cultivation with a plow, which leads to a reduction in the number of large-sized biopores with simultaneous soil loosening, which again facilitates root proliferation in the bulk soil (Dal Ferro et al., 2014; Edwards et al., 1988; Golabi et al., 1995; Holland, 2004). In our simulations, we therefore only considered biopores in the subsoil. Considering that anecic earthworms can burrow as deep as 2.5 m under favorable conditions (Kobel-Lamparski and Lamparski, 1987), biopores were considered to exist in the complete subsoil profile. To obtain biopores throughout the entire subsoil depth of 130 cm (Table 2), we inserted each biopore coordinate system 3.25 times, one below the other, into the soil grid, which resulted in 12 soil domains with individual biopore networks. Continuity of the biopore network across the connection of two biopore coordinate systems was obtained by vertically flipping one of the coordinate systems so that always either two top or two bottom ends were connected to each other (example in Fig. 3).

Root Hydraulic Properties

We used the values of the root hydraulic properties of wheat specified by Couvreur et al. (2014a), which are based on experimental measurements by Bramley et al. (2007), Sanderson et al. (1988), Tazawa et al. (1997), and Watt et al. (2008). Values for different root types as well as their variations with root age are represented in Fig. 4a and Fig. 4b for axial and lateral roots, respectively. Root hydraulic properties are key drivers of root water uptake by controlling the amount of water that can be transported from the soil to the root collar at a given time. They thus also substantially influence the model parameters of root system hydraulic conductance and relative distribution of root water uptake, which are used in the model approach by Couvreur et al. (2012).

Boundary Conditions for Simulation of Soil Water Flow, Root System Development, and Root Water Uptake

The boundary conditions at the top and bottom of the soil domain were set to time-variable flux and unit hydraulic gradient, respectively. The time-variable flux at the top boundary was calculated from the daily climatic water balance, which is defined as the difference between precipitation and evaporation. Additionally, we considered transpiration from the root collar. The simulation runtime was set to 112 d, i.e., the whole cropping cycle of spring wheat. Daily precipitation measurements were obtained from the climate station Klein-Altendorf; daily potential reference evapotranspiration ET_0 was estimated with the Penman–Monteith equation (Allen et al., 1998) from temperature, wind speed, relative humidity, and radiation measurements that were also obtained from the climate station Klein-Altendorf. Potential crop evapotranspiration ETc_{pot} [L T^{-1}] was estimated from ET_0 [L T^{-1}] using the single crop coefficient approach (Allen et al., 1998):

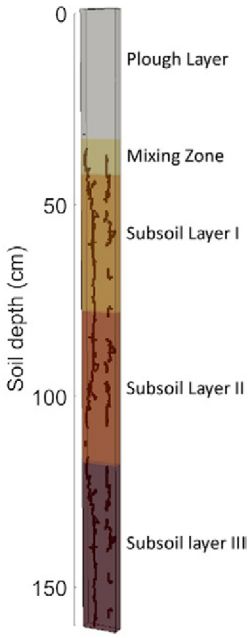

Fig. 3. Soil domain with five different soil layers (Table 2) and subsoil biopore system.

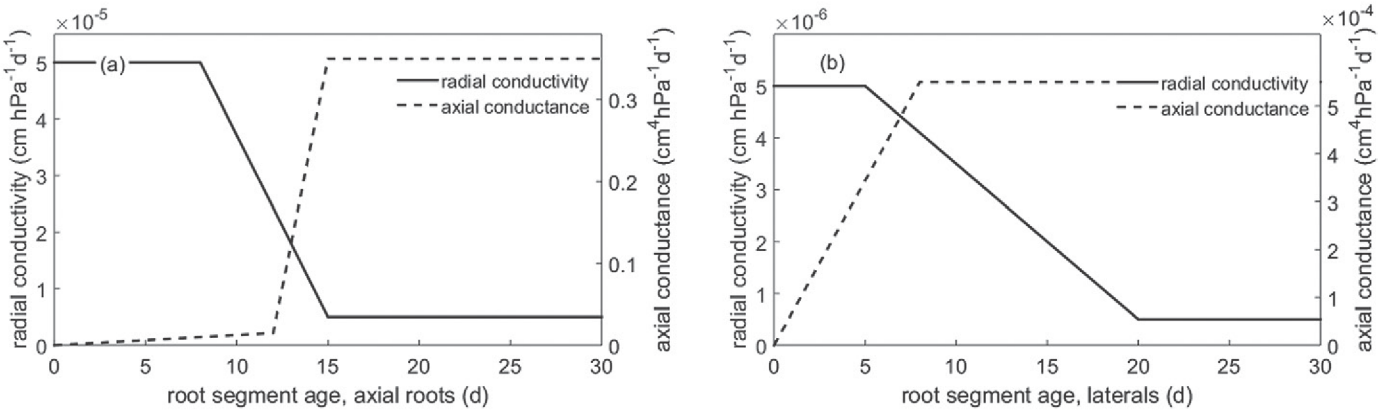

Fig. 4. Root hydraulic properties of spring wheat for (a) axial and (b) lateral root segments.

$$ETc_{pot} = k_c \times ET_0 \quad [12]$$

where k_c (dimensionless) is the crop coefficient. Crop coefficient values for spring wheat were derived for each crop stage (initial stage, midseason, and late stage) from Allen et al. (1998) and are 0.3 for the initial period (8 Apr.–14 May 2010), 1.15 for midseason (9 June–15 July 2010), and 0.25 for the late stage (16–31 July 2010). Potential crop evapotranspiration was partitioned into evaporation and transpiration based on Beer's law, which uses canopy interception to separate solar radiation from the total energy budget (Ritchie et al., 1972; Klosterhalfen et al., 2017):

$$T_{pot,\,daily} = ETc_{pot}\left[1-\exp\left(-k\ LAI\right)\right] \quad [13]$$

$$E_{pot,\,daily} = ETc_{pot}\exp\left(-k\ LAI\right) \quad [14]$$

where $T_{pot,daily}$ and $E_{pot,daily}$ are daily potential transpiration and evaporation fluxes [L T^{-1}], respectively, LAI is the leaf area index, which was measured in the field experiment (Table 1), and k is a constant governing the radiation extinction by the canopy (dimensionless) as a function of sun angle and the plant and leaf distribution (following Mo and Liu [2001], we used $k = 0.6$). Figure 5a shows precipitation, potential evaporation, and transpiration as well as LAI during the whole simulation period in 2010. To obtain transpiration from the root collar, daily potential transpiration was multiplied with the surface area of the soil domain (30 cm^2). Following the approach by Couvreur et al. (2014a), we considered daily sinusoidal variations in $T_{pot,daily}$ using

$$T_{pot}(t) = T_{pot,daily}\left[\sin\left(\frac{2\pi t}{24}-\frac{\pi}{2}\right)+1\right] \quad [15]$$

where t (h) is the time after midnight.

As mentioned above, root growth was considered to be a function of soil temperature. Daily soil temperature values at five different depths (0, 5, 10, 20, and 50 cm) were obtained from the German Weather Service (2017) as well as from the climate station Klein-Altendorf; soil temperature patterns during the simulation period are shown in Fig. 5b.

To mimic field conditions, we assumed periodic boundaries in the horizontal direction for root growth, soil water flow, and root system fluxes. In that way, simulated roots and water fluxes that exit the soil domain on one side simultaneously enter it on the opposite side. The computation time step of the root growth model is constant and was set to 0.16 d, which is just small enough so that the maximum possible size of a root segment does not exceed one grid side length. The computation time step of the soil water flow model was set to 10^{-1} d. This time step, however, is adjustable and can be reduced to a minimum value of 10^{-5} d if no convergence is reached. Root growth and root water uptake models were provided

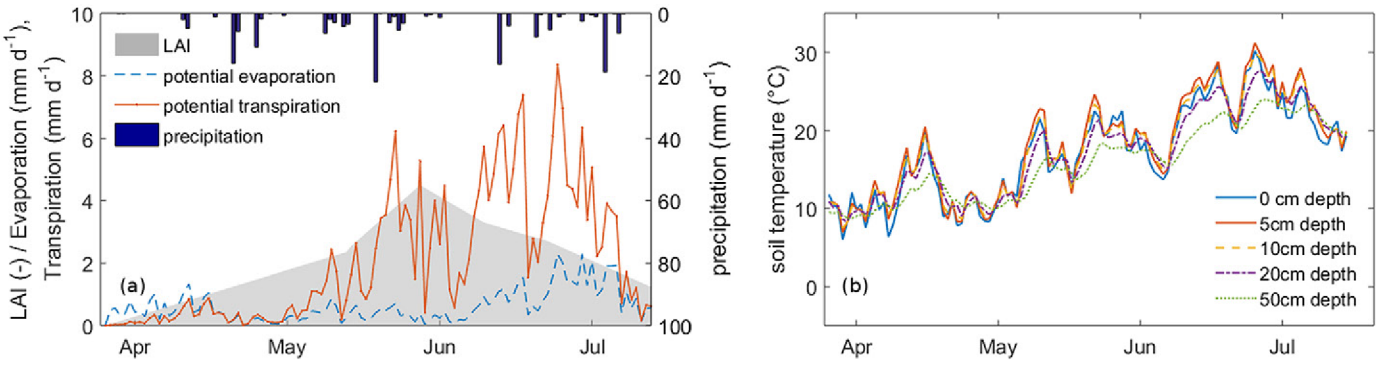

Fig. 5. (a) Leaf area index (LAI) for spring wheat, potential evaporation, potential transpiration, and precipitation and (b) soil temperature at five different depths during the whole simulation period from 8 April to 30 July 2010.

with updated root systems and SWP distributions, respectively, within the soil domain every day during the first 10 d of simulation, when the root systems changed rapidly due to large initial elongation rates, and every 5 d from Day 11 to Day 112, the last day of simulation. As initial conditions, the matric potential in the soil domain was set to hydrostatic equilibrium with −400 hPa at the top boundary.

Model Calibration via Optimization of Root Architecture Parameters

We used the model setup derived from the experimental field measurements as well as our 12 different biopore networks to simulate root systems during the entire cropping season of 112 d from 8 Apr. to 30 July 2010. To obtain realistic root system architectures, we optimized our root growth model input parameters so that simulated and experimentally observed RLDs in both bulk soil and biopores corresponded to each other. To indicate the quality of fit between observed and simulated RLDs, we computed Pearson's correlation coefficient R as well as the relative root mean square error (rRSME). While R is a measure of the statistical relationship between observed and simulated RLD, rRMSE defines the relative differences between observed and simulated RLD values (Loague and Green 1991). The parameter rRMSE was computed as

$$\mathrm{rRSME} = \left[\frac{1}{n}\sum_{i=1}^{n}\left(\mathrm{RLD}_{\mathrm{sim},i} - \mathrm{RLD}_{\mathrm{obs},i}\right)^2\right]^{1/2} \frac{100}{\overline{\mathrm{RLD}}_{\mathrm{obs}}} \qquad [16]$$

where n is the number of RLD measurements in a depth and $\mathrm{RLD}_{\mathrm{sim}}$ and $\mathrm{RLD}_{\mathrm{obs}}$ are simulated and observed RLDs, respectively. For the optimization procedure, we selected those five input parameters that had the greatest impact on root length density variation. While number, emergence time, and initial growth rate of axial roots are the major determinants of total root length density, sensitivity to gravitropism as well as root tortuosity define the distribution of root length density within the soil profile. Additionally, we optimized the parameter "conductance in the macropore," which defines the degree of anisotropy of penetration resistance in the soil elements containing biopore walls and affects the probability of a root to continue growing within a biopore or to reenter the bulk soil (Landl et al., 2017). The values of the optimized parameters were on the same orders of magnitude as standard values found in the literature. All remaining root growth model input parameters were derived from the literature. Parameter values, literature sources, and literature-derived ranges for optimized parameters are indicated in Supplemental Table S1.

Setup of Simulation Scenarios

The initial model setup was based on measurements from the field experiment. For a more general evaluation of the impact of subsoil biopores on root growth and root water uptake under varying environmental and soil physical conditions, we additionally set up five different simulation scenarios.

Scenario I: Presence of Subsoil Biopores

To get a better understanding of the impact of biopores on root system development and root water uptake, we performed simulations with and without subsoil biopores.

Scenario II: Subsoil Bulk Density

The importance of biopores as root growth pathways typically increases with soil compaction. We therefore additionally performed simulations with subsoil bulk density that was increased to 1.65 g cm^{-3}.

Scenario III: Influence of Partial Root–Soil Contact on Radial Root Hydraulic Conductivity

It has been suggested that root hairs may bridge the gap between soil and roots in biopores so that partial root–soil contact does not reduce root radial hydraulic conductivity (Carminati et al., 2013; Wasson et al., 2012). This aspect was taken into account by additional simulations with unlimited root radial hydraulic conductivity in biopores.

Scenario IV: Soil Type

Typically, roots use biopores as preferential growth pathways to reach water resources at greater depths. Subsoil water availability, however, depends on the soil type. Apart from the original silt loam, we therefore also performed simulations with sandy loam. While silt loam is characterized by a relatively high water holding capacity and hydraulic conductivity for a wide range of soil matric potentials, sandy loam is highly conductive close to saturation but rapidly becomes resistive to water flow when soil water potential decreases. These differences in soil hydraulic properties also lead to differences in SWP distributions in the soil domain, which in turn affect root system development. Water retention curves and soil hydraulic parameters used in our simulations are shown in Supplemental Fig. S1 and Tables S2 and S3.

Scenario V: Climatic Conditions

We performed additional simulations with climate data from 2012 measured at the same reference field site in Klein-Altendorf, Germany. As in 2010, the field plots were planted with spring wheat and we used measured LAI values to partition evapotranspiration into evaporation and transpiration. We used the crop coefficient values from the basic setup from 2010. Compared with 2010, 2012 was less dry, especially toward the end of the cropping season.

Using the optimized root architecture parameters, we simulated root growth and root water uptake for all possible combinations of soil physical and environmental conditions. Altogether, we performed simulations with 24 different setups, which is the factorial combination of three types of soil structure (biopores with limited hydraulic conductivity, no biopores, and biopores with unlimited hydraulic conductivity), two different soil bulk densities, two soil types, and climate data for two different seasons. For each of these setups, we ran simulations with all 12 different biopore systems; for combinations without biopores,

12 replicate simulations were performed. Altogether we therefore performed 24 × 12 = 288 different simulations.

Results

Comparison of Observed and Simulated Root Systems

Simulated RLD profiles could be well fitted to measured ones for all five observation dates via optimization of root growth model input parameters (Fig. 6). While the agreement between simulated and measured RLD profiles was quite good for root growth in the bulk soil (R = 0.84–0.94, rRMSE = 30–53%), less consistency was reached for the highly variable RLD profiles of root growth in biopores, where R was partly negative and rRMSE values were larger (R = −1–0.86, rRMSE = 43–142%). On the last measurement date, 46% of observed and 41% of simulated spring wheat RLD was accumulated in the topsoil and thus 54 and 59%, respectively, in the subsoil. The share of subsoil RLD in biopores relative to total subsoil RLD at the last day of measurement amounted to approximately 10% in observations and 9% in simulations. Considering that mean subsoil bioporosities in the simulation domain amount to approximately 10% (Table 3), this value appears very low; however, it must be noted that simulated lateral roots, which constitute the largest part of RLD, are generally not located within biopores due to plagiotropism (tendency to bend horizontally). If only axial roots are considered, the simulated share of subsoil RLD in biopores relative to total subsoil RLD amounts to 24%, which shows that simulated roots predominantly did use biopores as preferential growth paths. Observed and simulated maximum RLD in biopores within one soil layer at the 10-cm depth was similar, with values of 0.28 and 0.26 cm cm^{-3} that were recorded at 68 and 112 d after sowing (DAS). The maximum share of RLD in biopores relative to total RLD within one soil layer at the 10-cm depth amounted to 25 and 13% for observations and simulations, respectively; if only axial roots are considered, the simulated share increases to 40%.

Experimentally observed RLD profiles show that topsoil layers also contain a low share of roots growing in biopores. Our simulations could not reproduce these observations because biopores were only considered in the subsoil. Between the two-node and dough stage (DAS 54–97), simulated rooting depths were larger than experimentally observed ones because RLDs were measured only down to a depth of 80 cm. At the first four measurement dates, experimentally observed RLDs in biopores were substantially larger than simulated RLDs in biopores. This is due to inconsistencies in observed biopore RLDs: summed across all depths, observed RLDs in biopores were larger at DAS 68 than 6 wk later at DAS 112, even though RLDs in the bulk soil

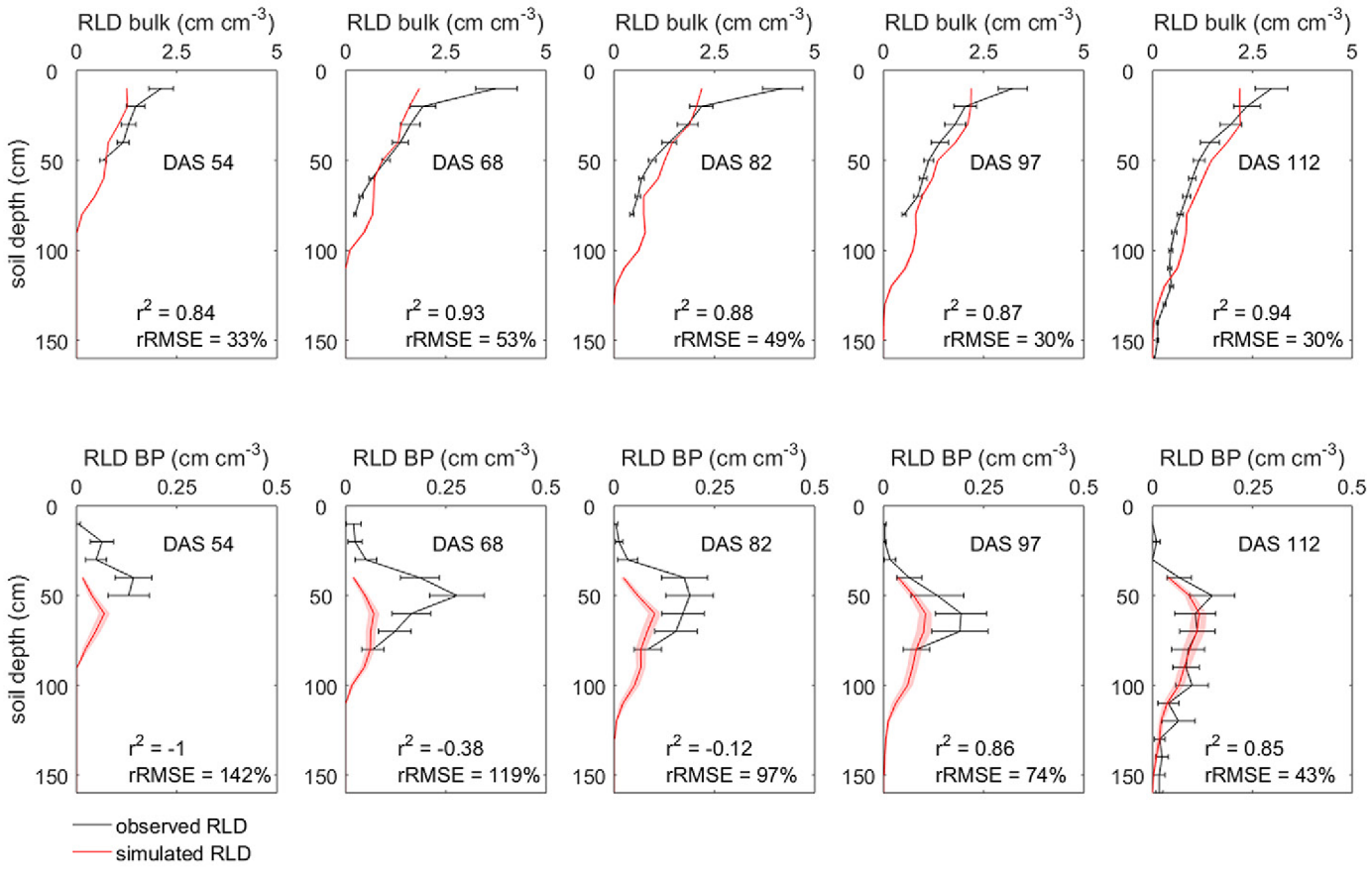

Fig. 6. Measured and simulated root length density (RLD) in bulk soil and biopores (BP) at five different points in time. Error bars and shaded areas (partly invisible due to low variance) represent the standard error of the mean (measured RLD: n = 280; simulated RLD: n = 12).

increased with time. In our simulations, however, RLDs in biopores obviously increased with increasing RLDs in the bulk soil. Considering that for each point in time a new soil profile is used to count roots with the profile wall method, these inconsistencies in observed RLDs can be regarded as the natural variability of root growth in biopores.

Simulated roots generally showed lower RLD in the uppermost topsoil layer. This is a model artifact, which is caused by our assumption of constant gravitropism for axial roots. Axial roots that emerge from the seed therefore immediately start bending toward the vertical and do not spread out horizontally. Our simulations also failed to reproduce the observed increase in topsoil RLD until flowering (DAS 82) and the decrease thereafter because our root architecture model does not take into account root decay. However, considering that our main interest was root growth behavior in the subsoil, these deviations can be regarded as negligible.

The optimized values of root growth model input parameters, which were used for further root architecture simulations, were all within the range of values found in the literature and are listed together with reference sources in the Supplemental Material.

Influence of Biopores on Simulated Root Length Density under Different Soil Physical and Environmental Conditions

Figure 7 shows maximum rooting depths as well as total RLD (total root length scaled with the volume of the soil domain) on the last day of simulation (DAS 112) averaged across 12 individual simulation runs with different biopore networks and without biopores for scenario combinations with low and high soil bulk density, silt and sandy loam, and climate conditions of 2010 and 2012.

For all different environmental and soil physical conditions, biopores led to an increase in rooting depth (between 13 and 35% at 16 and 27 cm, respectively) and total RLD (between 10 and 14% for 0.06 and 0.12 cm cm^{-3}, respectively). The increase in rooting depth was stronger for high than for low soil bulk density (both in relative and absolute numbers). This is caused by the stronger difference between bulk soil and biopore penetration resistance in more compact soil, which causes more axial roots to remain within biopores and to grow along them. Different soil types and climate conditions did not lead to substantially different increases in rooting depth. In contrast to rooting depth, the biopore-affected increase in total RLD was larger for low than for high soil bulk density because lateral roots, which generally left the biopore and reentered the bulk soil due to their tendency to bend horizontally, developed faster in loose than in hard bulk soil. In more compact soil, biopores mainly facilitated axial root growth, while laterals that reentered the bulk soil needed longer time to fully develop. Different soil types and climate conditions did not lead to substantially different increases in total RLD.

Increased soil bulk density led to lower maximum rooting depths and lower total RLDs due to increased mechanical stress. Interestingly, both maximum rooting depth and total RLD were larger in sandy loam than in silt loam. This is caused by the different hydraulic properties of the two soils leading to differences in SWP and thus soil penetration resistance. The SWP heterogeneity was more pronounced in sandy loam than in silt loam due to the sandy loam's larger hydraulic resistivity under the prevailing soil water contents. The SWP in sandy loam was therefore more negative in upper soil layers and less negative in deeper soil layers compared with silt loam. The SWP-triggered impedance of root tip elongation in deeper soil layers was then stronger in silt loam than in sandy loam. It must also be noted that water contents are higher in silt loam than in sandy loam in the case of equal SWP. Despite the silt loam's larger saturated water content, this leads to a higher degree of saturation and thus to larger soil penetration resistance values and lower root elongation rates in silt loam than in sandy loam at equal SWP (Eq. [5]). Differences in climate conditions between 2010 and 2012, which mostly appeared in the second half of the growing period, were not large enough to substantially influence maximum rooting depths or total RLDs.

It must be noted that despite the presence of biopores, the maximum rooting depth in dense soil was lower than the maximum rooting depth in loose soil, which indicates that roots did not grow within biopores throughout the entire subsoil depth. The reasons are biopore discontinuities within the soil depth and the tendency of roots to leave non-vertically oriented biopores.

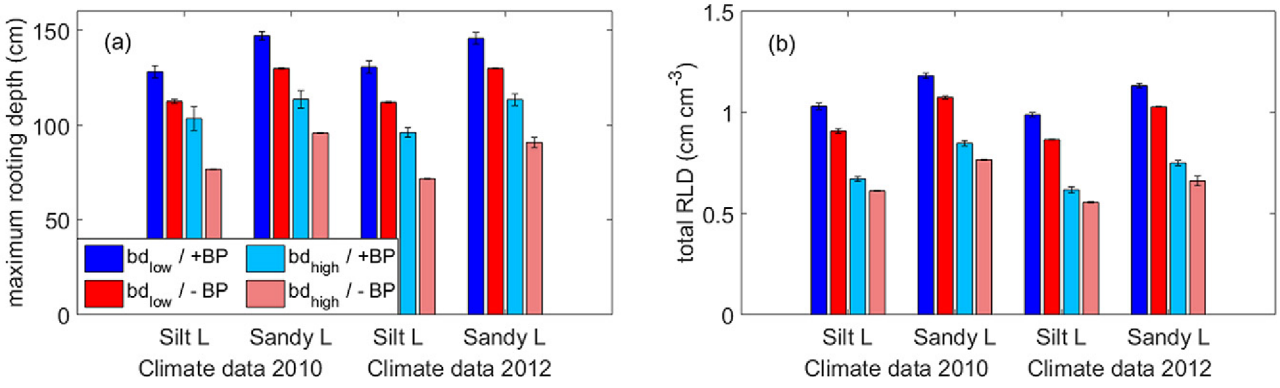

Fig. 7. (a) Maximum rooting depth and (b) total root length density (RLD) on the last day of simulation (112 d after sowing) for root growth in soil with and without biopores (±BP), at low (bd_{low}) or high (bd_{high}) bulk density, in silt loam or sandy loam under the climatic conditions of 2010 and 2012. Error bars represent the standard error of the mean for 12 individual simulation runs.

Influence of Biopores on Root Hydraulic Architecture Parameters

We computed root hydraulic architecture parameters for all possible combinations of soil physical and environmental conditions and the various biopore systems. Mean root system conductance K_{rs}, which describes the water flow per unit of water potential difference between root collar and soil, is a function of root system size and root hydraulic parameters (radial and axial root conductance, Fig. 4). Under the assumption of limited hydraulic conductivity (HC) of the root–soil interface in biopores, the mean root system conductance is furthermore a function of root–soil contact. When assuming limited HC in biopores, the increase in root system conductance due to increased root system size was partly cancelled out by its decrease due to incomplete root–soil contact. When assuming unlimited HC in biopores, root system conductance was naturally higher than in simulations without biopores due to increased root system size. These relationships persisted for simulation scenarios with different soil types and climate conditions and are represented for scenario combinations with silt loam and climate conditions of 2010 in Fig. 8a. Absolute values of root system conductance were higher for sandy loam than for silt loam due to larger root systems.

The standard sink fraction, SSF, defines the location from which a root takes up water. To explore the influence of biopores on SSF, we use the measure "mean depth of the standard sink fraction" (zSSF), which is defined as the product of SSF and the depth of the respective root segment summed across all segments. Biopores led to an increase in rooting depth in both low and high soil bulk density and therefore also to an increase in zSSF. When assuming limited HC in biopores, the increase in zSSF was less pronounced (Fig. 8b). This was true for all simulation scenarios with different soil types and climate conditions and is represented for scenario combinations with silt loam and climate conditions of 2010 in Fig. 8b. Absolute values of zSSF were higher in sandy loam than in silt loam due to deeper reaching root systems.

An important physiological parameter is the carbon cost of the root biomass. Root water uptake efficiency can thus be described by the ability of a plant to take up water per gram of carbon spent in the root system. We found varying results for the influence of biopores on root water uptake efficiency (Fig. 8c). Up to a certain root system volume (corresponding to a certain root system age), root water uptake efficiency was similar for simulations with and without biopores. For larger root system volumes (older root systems), however, biopores led to larger water uptake efficiency in simulations with unlimited and—to a lesser extent—also with limited HC in biopores. These relationships persisted for simulation scenarios with different soil types and climate conditions and are represented for scenario combinations with silt loam and climate conditions of 2010 in Fig. 8c.

Influence of Biopores on Root Water Uptake

Daily cumulated transpiration (Fig. 9) as well as mean daily equivalent SWP sensed by the plant (Fig. 10) was computed for all possible combinations of soil physical and environmental conditions and the various biopore systems. During the second part of the reference season 2010 (mid-May to mid-July), a pronounced dry period led to significant plant drought stress, and transpiration demands could no longer be satisfied (Fig. 9a, 9b, 10a, and 10b). Under these conditions, simulations with biopores led to higher actual transpiration rates than simulations without biopores and thus to a better plant water supply in both loose and dense soil. Interestingly, at the beginning of the dry period, simulations with limited HC showed lower transpiration rates than simulations with unlimited HC; toward the end of the dry period, however, the situation changed and simulations with limited HC revealed equal or even slightly higher transpiration rates than simulations with unlimited HC (Fig. 9a and 9b). Unlimited HC in biopores and thus higher root system conductance is therefore only an advantage for plant water uptake as long as soil water availability is high enough. This phenomenon is also reflected in the plant-sensed SWPs, which differ at the beginning, but are similar at the end of the dry period for simulations with limited and unlimited HC (Fig. 10a and 10b). Despite larger root systems and thus larger root system conductances, actual transpiration rates were lower

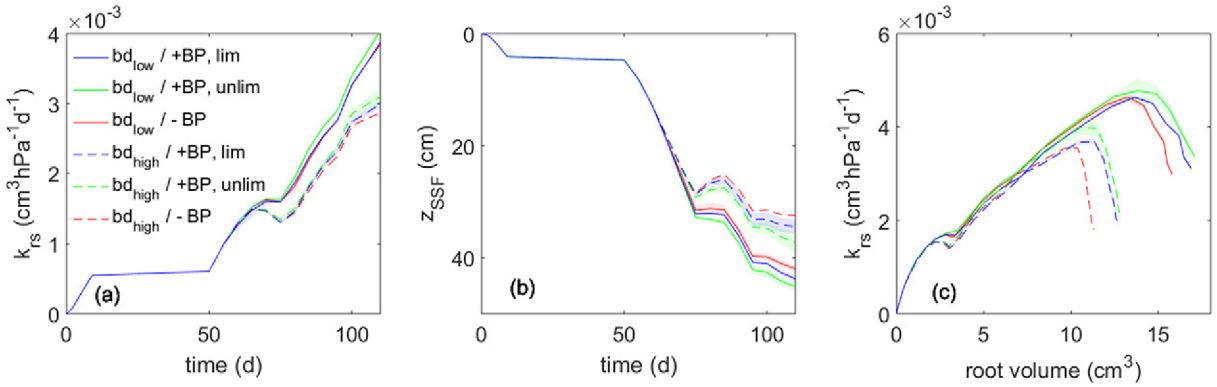

Fig. 8. Evolution of (a) mean root system conductance (k_{rs}) and (b) depth of the standard sink fraction (z_{SSF}) with time; (c) relationship between k_{rs} and root volume with and without biopores (±BP), at low (bd_{low}) or high (bd_{high}) bulk density, and with unlimited (unlim) or limited (lim) radial root hydraulic conductivity for a silt loam soil under the climatic conditions of 2010. Each line is the average of 12 individual simulation runs; the shaded bands (partly invisible due to low variance) represent the 95% confidence interval.

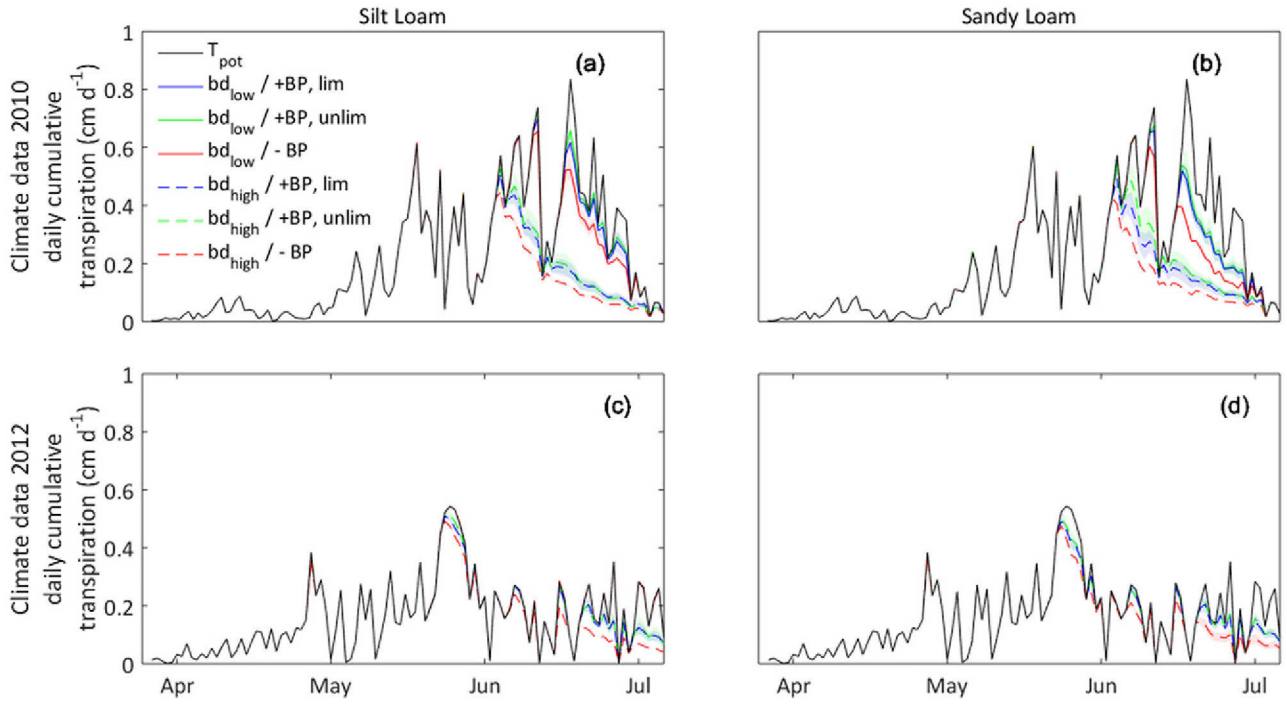

Fig. 9. Daily potential (T_{pot}) and actual transpiration rates during the entire growing period for (a) climate data of 2010 and silt loam soil , (b) climate data of 2010 and sandy loam soil, (c) climate data of 2012 and silt loam soil, and (d) climate data 2012 and sandy loam soil with and without biopores (±BP), at low (bd_{low}) or high (bd_{high}) bulk density, and with unlimited (unlim) or limited (lim) radial root hydraulic conductivity. Each line is the average of 12 individual simulation runs; the shaded bands (partly invisible due to low variance) represent the 95% confidence interval.

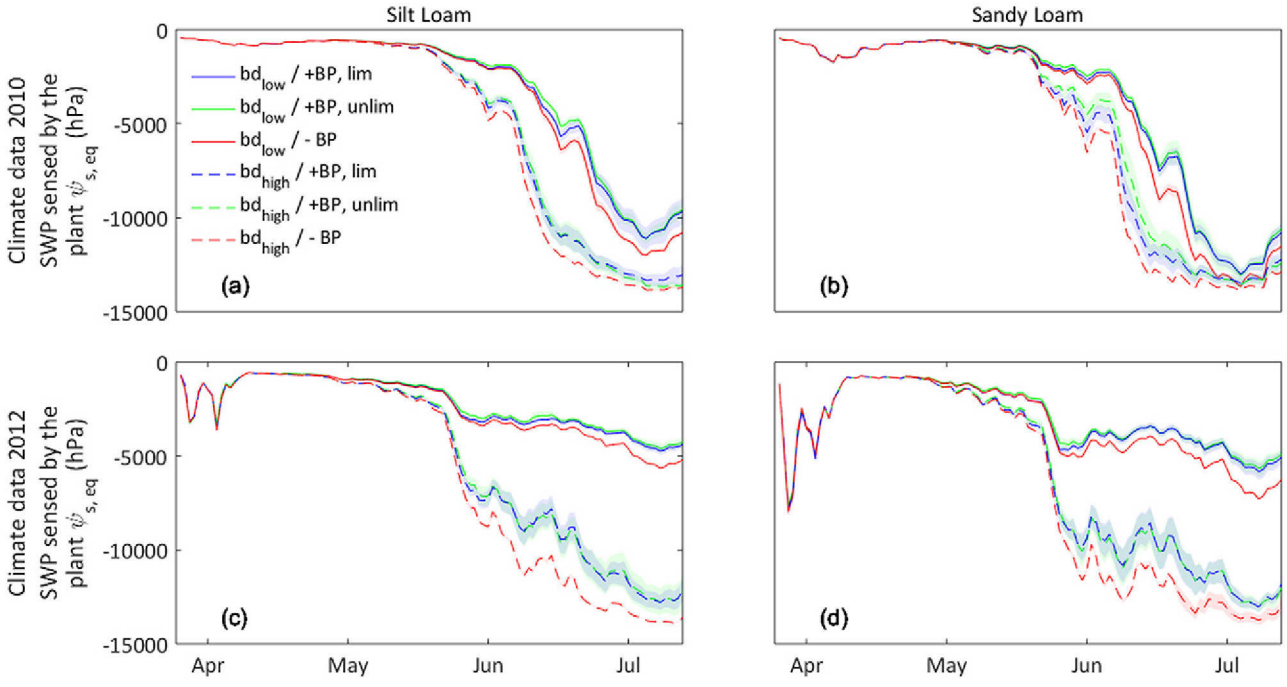

Fig. 10. Mean soil water potential (SWP) sensed by the plant at each day of the growing period for (a) climate data of 2010 and silt loam, (b) climate data of 2010 and sandy loam, (c) climate data of 2012 and silt loam and (d) climate data of 2012 and sandy loam with and without biopores (±BP), at low (bd_{low}) or high (bd_{high}) bulk density, and with unlimited (unlim) or limited (lim) radial root hydraulic conductivity. Each line is the average of 12 individual simulation runs; the shaded bands (partly invisible due to low variance) represent the 95% confidence interval.

in loose sandy loam than in loose silt loam. This is caused by the sandy loam's more negative SWP in the medium to upper soil layers (~0–80 cm) where root water uptake predominantly takes place due to higher RLD in this soil region (cf. zSSF, Fig. 8b) and is also reflected in the plant-sensed SWPs, which are more negative for loose sandy loam than for loose silt loam (Fig. 10a and 10b). In dense soil, silt loam and sandy loam showed similar transpiration rates because SWPs in the upper soil layers where root water uptake took place were equally negative for both soil types (Fig. 10a and 10b). Simulations with the climate conditions of spring 2012 led to optimal root water uptake in loose soil throughout the entire growing season and to less drought stress for plants growing in dense soil. Simulations with biopores again led to less negative equivalent SWP sensed by the plant and thus to larger actual transpiration rates compared with simulations without biopores. Actual transpiration rates were slightly higher for silt loam than for sandy loam due to slightly less negative SWPs in the uppermost soil layers (Fig. 9c, 9d, 10c, and 10d).

To better understand the impact of biopores on total root water uptake throughout the entire growing season, we evaluated cumulated transpiration deficits (Fig. 11). Simulations with biopores led to lower transpiration deficits than simulations without biopores for any climate and soil physical condition and for limited and unlimited HC in biopores. The impact of biopores on transpiration deficits was larger in dense soil than in loose soil. This is a result of both the generally larger transpiration deficits produced by smaller root systems and the larger effect of biopores on rooting depth. Biopores also had a larger effect on transpiration deficits in sandy loam than in silt loam. This was caused by the larger SWP variation with depth in sandy loam, which increases the importance of root water uptake from deeper, wetter soil layers to satisfy transpiration demands. In loose soil, transpiration deficits were reduced by up to 14 mm (season 2010, sandy loam), which represented 7% of the seasonal transpiration demand. In dense soil, transpiration deficits were reduced by up to 24 mm (season 2010, sandy loam), which represented 11% of the seasonal transpiration demand.

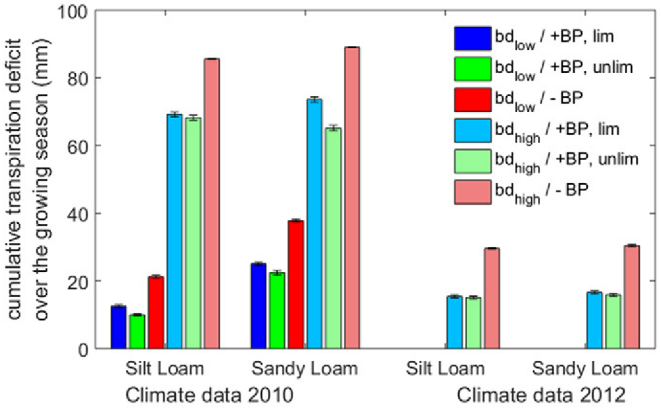

Fig. 11. Transpiration deficit cumulated during the entire growing season with and without biopores (±BP), at low (bd_{low}) or high (bd_{high}) bulk density, and with unlimited (unlim) or limited (lim) radial root hydraulic conductivity. Error bars represent the standard error of the mean for 12 individual simulation runs.

Discussion

Modeling Root Growth in Soil with Biopores

Via optimization of root growth model input parameters, we were able to simulate RLD profiles in the bulk soil and biopores that corresponded well to experimentally observed ones. All optimized model input parameters were in the range of values found in the literature (Supplemental Table S1). Our parameterized simulation model was able to reproduce the impacts of biopores on root system development as described in the literature (Hirth et al., 2005; Stirzaker et al., 1996), in which biopores led to substantial increases in both total root length and rooting depth and the latter phenomenon increased for more compact soil. These results suggest that our simulated root systems represent a valid basis for further analysis of root water uptake under different soil physical and environmental conditions. To improve model simulation of root development in biopores for different soils as well as under varying environmental conditions, however, more quantitative information from both field and laboratory experiments will be necessary.

At our study site, the abundance of subsoil biopores was observed to decrease with soil depth (Athmann et al., 2013; Perkons et al., 2014), which is in line with most studies from the literature (e.g., White and Kirkegaard, 2010; Pitkänen and Nuutinen, 1997). However, other studies (e.g., da Silva et al., 2016) have reported constant or increasing numbers of subsoil biopores with soil depth or a homogeneous distribution of biopores in a soil depth of 125 to 150 cm (Nielsen et al., 2010). In the present study, we used a homogeneous biopore network throughout the entire subsoil profile, which we considered to be justified for a general evaluation of the impact of biopores on root growth and root water uptake. For a more detailed evaluation, however, differences in subsoil biopore density with depth need to be taken into account. The abundance of biopores in the topsoil is known to largely depend on the tillage practice. While conventional tillage leads to soft topsoil with only a few biopores, no-till management results in more compact topsoil with a large number of biopores (Dal Ferro et al., 2014; Golabi et al., 1995; Holland, 2004). Crop development simulation under no-till practice thus further requires the consideration of topsoil biopores, which can be expected to yet again increase the impact of biopores on root growth and root water uptake.

For reasons of simplicity and a lack of accurate values, we assumed regular branch spacing and constant lateral root length under any soil physical condition. Bao et al. (2014), however, observed that lateral root formation depends on the availability of water in the vicinity of the root, which might be of importance for root branching within biopores due to the prevailing limited root–soil contact. Lateral root length, on the other hand, was observed to decrease under soil compaction (Grzesiak, 2009; Konôpka et al., 2009), which can be expected to result in different lengths of

laterals that develop within a biopore and those that grow back into the bulk soil.

The mean share of subsoil RLD in biopores relative to total subsoil RLD observed in the field experiment amounted to 10% on the last day of measurement, which is rather low compared with values from the literature, where shares of 14 to 100% have been reported (Ehlers et al., 1983; Gaiser et al., 2013; Nakamoto, 2000; White and Kirkegaard, 2010). The reasons for this large variability in biopore RLD observed in different studies are manifold and include crop species, soil structure and texture, but above all diverging definitions of biopores with regard to diameter as well as different methods to assess the root distribution within the bulk soil and biopores (e.g., profile wall method, Böhm and Koepke, 1977; core-break method, Kirkegaard et al., 2007). In our simulations, the low share of subsoil RLD in biopores relative to the total subsoil RLD is mainly due to the fact that in our model, lateral roots are hardly ever located within biopores. Based on findings by Cuesta et al. (2013) and Rosquete et al. (2013), we considered lateral roots to be influenced by plagiotropism and to predominantly grow in a horizontal direction. Simulated lateral roots therefore left the generally vertically oriented pores by reentering the bulk soil and hence did not contribute to the share of subsoil biopore RLD. If only axial roots were considered, the simulated share of subsoil RLD in biopores relative to total subsoil RLD would increase from 9 to 24% in loose soil and from 9 to 26% in dense soil. In the field, Athmann et al. (2013) observed that the growth behavior of lateral roots in biopores depends on the crop root architecture. The share of laterals reentering the bulk soil, however, could not be quantified in these field experiments. An interesting question is whether lateral roots in biopores premeditatedly grow toward the bulk soil to gain better access to water and nutrient resources. Such feedforward mechanisms, where plants are able to "sense" their physical environment, have been observed in several studies (e.g., Colombi et al., 2017; Passioura, 2002; Stirzaker et al., 1996).

Our model was well capable of reproducing experimental observations of root system development in soil with biopores, but it also showed limitations. The assumption of lateral periodic boundaries allowed us to mimic field conditions with regard to root growth and water flow; however, the biopore system was not periodic in the lateral direction. A root that grew along a biopore and reached the border of the soil domain was therefore obliged to grow out of the biopore and to reenter the bulk soil (Fig. 12–1). Another limitation was posed by the cubic grid cell structure of the biopore system: root growth direction is computed in accordance with Eq. [2] as the product of the soil mechanical conductance tensor and a driving force, which is influenced by the previous growth direction, a random deflection angle, and gravitropism. To grow around the corner of a cubic grid cell, a root has to endure large direction changes, i.e., the direction of the mechanical conductance tensor must dominate the direction of the driving force. If the bulk soil is not entirely impenetrable, roots therefore frequently reenter the bulk soil instead of continuing to grow along biopores (Fig. 12–2). Furthermore, we know from experimental

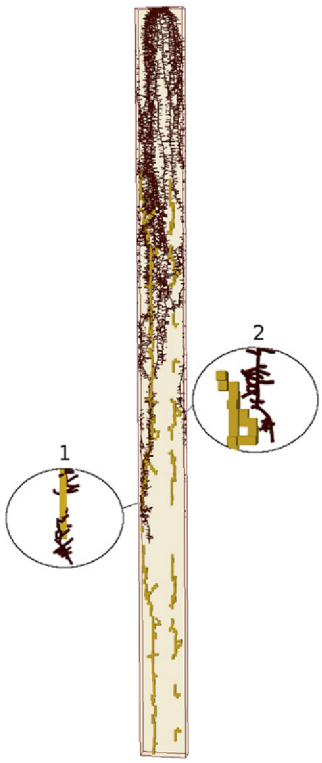

Fig. 12. Simulated root system (brown) in soil with biopores (yellow): root growing out of discontinuous biopore (1), and root leaving biopore that is not vertically aligned (2).

studies that biopore walls are generally more compact than the surrounding bulk soil (Stirzaker et al., 1996; Young, 1998), which means that roots are less likely to leave a pore when already inside. Our model, though, does not take into account biopore wall compaction. The greatest model limitation, however, was implied by the spatial resolution of the model. The relatively coarse resolution, which was necessary to meet computational requirements, led to bioporosities that were much larger than those observed in the field. By adjusting root growth model parameters, we were able to simulate RLDs in biopores that were comparable to those observed. However, this implies that model parameterization is sensitive to spatial model resolution. To solve this issue, further research and model development but also computing power is needed.

Several studies have shown that biopores play an important role with regard to soil aeration (Tracy et al., 2011; Bengough et al., 2011). Uteau et al. (2013) reported for the site in Klein-Altendorf that alfalfa increased air capacity, air permeability, and diffusion coefficients in the subsoil, while fescue, with its shallower root system, did not affect subsoil structure and hence soil aeration. In other studies, compacted soils with poor pore structure were found to be prone to waterlogging, which causes hypoxia and in consequence limits root elongation (Bengough et al., 2011). The beneficial effect of biopores for root growth can thus be assumed to be even greater if poor soil aeration its effective hypoxia were additionally considered as a limiting factor for root system development.

Legumes were shown to be more sensitive to soil compaction than cereals (Arvidsson and Håkansson, 2014), and soybean [*Glycine max* (L.) Merr.], maize, and barley roots were observed to colonize biopores more frequently than wheat roots when grown on the same field site (Colombi et al., 2017; Perkons et al., 2014). The significance of biopores as root growth pathways to greater soil depths may thus be even higher for plants other than wheat.

Modeling Root Water Uptake in Soil with Biopores

In times of drought, our simulations showed a beneficial impact of biopores on root water uptake. Biopores could thereby reduce a transpiration deficit by up to 24 mm, which represents 11% of the seasonal transpiration demand of spring wheat in our study area. This positive effect was primarily caused by the increased rooting depth in structured soil, which allowed roots to take up water from deeper and wetter soil regions.

The impact of biopores on hydraulic root architecture parameters depended on the water uptake ability of roots with limited root–soil contact. When unlimited hydraulic conductivity at the root–biopore wall interface was assumed, mean root water uptake took place deeper in the soil domain and root system conductance increased. When limited hydraulic conductivity at the root–biopore wall interface was assumed, roots were also able to take up water from deeper soil layers but root system conductance remained fairly constant. These findings may be important for simulations of root water uptake in structured soil using one-dimensional models (e.g., HYDRUS, Šimůnek et al., 2016) where the impact of biopores on plant transpiration can be taken into account only implicitly via root hydraulic architecture parameters and root length density profiles.

Many studies (e.g., Stirzaker et al., 1996; White and Kirkegaard, 2010; Passioura, 2002) have emphasized the problem of poor root–soil contact in biopores and its adverse effect on root water uptake and plant development. However, simulations with limited HC at the root–soil interface in biopores performed better in meeting plant transpiration demands than simulations without biopores under any soil physical and environmental condition. Furthermore, toward the end of dry periods when the soil was already water depleted, simulations with limited HC in biopores led to equal or even slightly higher actual transpiration rates than simulations with unlimited HC in biopores. Similar results were found by Meunier et al. (2016) and Couvreur et al. (2014b), who showed that root systems with low radial conductance can maintain higher transpiration rates toward the end of a dry period.

Our simulation results suggest that the influence of biopores on root water uptake differs for different soil densities as well as soil types. Due to the larger increase in rooting depth, biopores had a more beneficial effect on root water uptake in more compact soil. Furthermore, the effect of biopores was stronger in sandy loam than in silt loam due to the sandy loam's higher soil hydraulic resistivity at low soil water potentials. When evaluating the impact of biopores on crop performance, it is therefore necessary to take into account not only characteristics that are directly related to biopores (e.g., number of biopores per unit surface area and the abundance and spatial distribution of roots in biopores) but also properties whose connection to biopores is less evident, such as soil type and soil bulk density.

In the present study, we considered biopores to be air filled at all times. Under natural conditions, however, rain events can lead to preferential flow in biopores, which significantly influences the water content distribution in the soil profile (Jarvis et al., 2016). Preferential flow allows water to quickly infiltrate and drain into deeper soil layers and thereby reduces the amount of water that can be stored in the topsoil (Good et al., 2015). This difference in water distribution within the soil profile is encountered by larger rooting depths due to biopores.

Conclusion

In this simulation study, we combined extensive experimental field data with an explicit three-dimensional model for the simulation of water flow, root system development, and root water uptake in soil with biopores. Our model increases understanding of plant physiological responses to structured soil under different soil physical and environmental conditions. Our simulation results confirmed the beneficial impact of biopores for root penetration into greater soil depths as well as for plant transpiration under drought conditions. The positive influence of biopores persisted even under the assumption of reduced root water uptake in biopores due to limited root–soil contact and was larger for dense soil than for loose soil as well as for sandy loam than for silt loam. We furthermore evaluated the influence of biopores on root hydraulic architecture parameters. These relationships may be of use for larger scale simulations with one-dimensional models that can only implicitly take into account the effect of biopores on root growth and root water uptake via RLD profiles and root hydraulic architecture parameters.

Acknowledgments

This study was supported by the German Research Foundation (Deutsche Forschungsgemeinschaft) within the framework of the research consortium DFG PAK 888. We thank Sabine Seidel for the collection of the field data as well as the staff of the Campus Klein-Altendorf for providing the climate data.

References

Allen, R.G., L.S. Pereira, D. Raes, and M. Smith. 1998. Crop evapotranspiration: Guidelines for computing crop water requirements. Irrig. Drain. Pap. 56. FAO, Rome.

Arvidsson, J., and I. Håkansson. 2014. Response of different crops to soil compaction: Short-term effects in Swedish field experiments. Soil Tillage Res. 138:56–63. doi:10.1016/j.still.2013.12.006

Athmann, M., T. Kautz, R. Pude, and U. Köpke. 2013. Root growth in biopores: Evaluation with in situ endoscopy. Plant Soil 371:179–190. doi:10.1007/s11104-013-1673-5

Bao, Y., P. Aggarwal, N.E. Robbins, C.J. Sturrock, M.C. Thompson, H.Q. Tan, et al. 2014. Plant roots use a patterning mechanism to position lateral root branches toward available water. Proc. Natl. Acad. Sci. 111:9319–9324. doi:10.1073/pnas.1400966111

Barej, J.A.M., S. Pätzold, U. Perkons, and W. Amelung. 2014. Phosphorus fractions in bulk subsoil and its biopore system. Eur. J. Soil Sci. 65:553–561. doi:10.1111/ejss.12124

Bengough, A., B. McKenzie, P. Hallett, and T. Valentine. 2011. Root elongation, water stress, and mechanical impedance: A review of limiting stresses and beneficial root tip traits. J. Exp. Bot. 62:59–68. doi:10.1093/jxb/erq350

Bengough, A.G., and C.E. Mullins. 1990. Mechanical impedance to root growth: A review of experimental techniques and root growth responses. Eur. J. Soil Sci. 41:341–358. doi:10.1111/j.1365-2389.1990.tb00070.x

Böhm, W., and U. Koepke. 1977. Comparative root investigations with two profile wall methods. Z. Acker- Pflanzenbau 144:297–303.

Bramley, H., N.C. Turner, D.W. Turner, and S.D. Tyerman. 2007. Comparison between gradient-dependent hydraulic conductivities of roots using the root pressure probe: The role of pressure propagations and implications for the relative roles of parallel radial pathways. Plant Cell Environ. 30:861–874. doi:10.1111/j.1365-3040.2007.01678.x

Cai, G., J. Vanderborght, V. Couvreur, C.M. Mboh, and H. Vereecken. 2018. Parameterization of root water uptake models considering dynamic root distributions and water uptake compensation. Vadose Zone J. 17:160125. doi:10.2136/vzj2016.12.0125 [erratum: 17:170201. doi:10.2136/vzj2017.11.0201er]

Carminati, A., D. Vetterlein, N. Koebernick, S. Blaser, U. Weller, and H.-J. Vogel. 2013. Do roots mind the gap? Plant Soil 367:651–661. doi:10.1007/s11104-012-1496-9

Chen, Y.L., J. Palta, J. Clements, B. Buirchell, K.H. Siddique, and Z. Rengel. 2014. Root architecture alteration of narrow-leafed lupin and wheat in response to soil compaction. Field Crops Res. 165:61–70. doi:10.1016/j.fcr.2014.04.007

Clark, L.J., W.R. Whalley, and P.B. Barraclough. 2003. How do roots penetrate strong soil? Plant Soil 255:93–104. doi:10.1023/A:1026140122848

Clausnitzer, V., and J. Hopmans. 1994. Simultaneous modeling of transient three-dimensional root growth and soil water flow. Plant Soil 164:299–314. doi:10.1007/BF00010082

Colombi, T., N. Kirchgessner, A. Walter, and T. Keller. 2017. Root tip shape governs root elongation rate under increased soil strength. Plant Physiol. 174:2289–2301. doi:10.1104/pp.17.00357

Colombi, T., L.C. Torres, A. Walter, and T. Keller. 2018. Feedbacks between soil penetration resistance, root architecture and water uptake limit water accessibility and crop growth: A vicious circle. Sci. Total Environ. 626:1026–1035. doi:10.1016/j.scitotenv.2018.01.129

Couvreur, V., L. Beff, and M. Javaux. 2014a. Horizontal soil water potential heterogeneity: Simplifying approaches for crop water dynamics models. Hydrol. Earth Syst. Sci. 18:1723–1743. doi:10.5194/hess-18-1723-2014

Couvreur, V., J. Vanderborght, X. Draye, and M. Javaux. 2014b. Dynamic aspects of soil water availability for isohydric plants: Focus on root hydraulic resistances. Water Resour. Res. 50:8891–8906. doi:10.1002/2014WR015608

Couvreur, V., J. Vanderborght, and M. Javaux. 2012. A simple three-dimensional macroscopic root water uptake model based on the hydraulic architecture approach. Hydrol. Earth Syst. Sci. 16:2957–2971. doi:10.5194/hess-16-2957-2012

Cuesta, C., K. Wabnik, and E. Benková. 2013. Systems approaches to study root architecture dynamics. Front. Plant Sci. 4:537. doi:10.3389/fpls.2013.00537

Dal Ferro, N., L. Sartori, G. Simonetti, A. Berti, and F. Morari. 2014. Soil macro- and microstructure as affected by different tillage systems and their effects on maize root growth. Soil Tillage Res. 140:55–65. doi:10.1016/j.still.2014.02.003

da Silva, F.R., J.A. Albuquerque, A. da Costa, S.M.V. Fontoura, C. Bayer, and M.I. Warmling. 2016. Physical properties of a Hapludox after three decades under different soil management systems. Rev. Bras. Cienc. Solo 40:e0140331. doi:10.1590/18069657rbcs20140331

de Moraes, M.T., A.G. Bengough, H. Debiasi, J.C. Franchini, R. Levien, A. Schnepf, and D. Leitner. 2018. Mechanistic framework to link root growth models with weather and soil physical properties, including example applications to soybean growth in Brazil. Plant Soil. doi:10.1007/s11104-018-3656-z

de Willigen, P., M. Heinen, and M. van Noordwijk. 2018. Roots partially in contact with soil: Analytical solutions and approximation in models of nutrient and water uptake. Vadose Zone J. 17:170060. doi:10.2136/vzj2017.03.0060

Dexter, A., and J. Hewitt. 1978. The deflection of plant roots. J. Agric. Eng. Res. 23:17–22. doi:10.1016/0021-8634(78)90075-6

Doussan, C., G. Vercambre, and L. Pagès. 1998. Modelling of the hydraulic architecture of root systems: An integrated approach to water absorption—Distribution of axial and radial conductances in maize. Ann. Bot. 81:225–232. doi:10.1006/anbo.1997.0541

Edwards, W.M., L.D. Norton, and C.E. Redmond. 1988. Characterizing macropores that affect infiltration into nontilled soil. Soil Sci. Soc. Am. J. 52:483–487. doi:10.2136/sssaj1988.03615995005200020033x

Ehlers, W., U. Köpke, E. Hesse, and W. Böhm. 1983. Penetration resistance and root growth of oats in tilled and untilled loess soil. Soil Tillage Res. 3:261–275. doi:10.1016/0167-1987(83)90027-2

IUSS Working Group WRB. 2014. World reference base for soil resources 2014: International soil classification system for naming soils and creating legends for soil maps. World Soil Resour. Rep. 106. FAO, Rome.

Fredlund, D.G., and A. Xing. 1994. Equations for the soil-water characteristic curve. Can. Geotech. J. 31:521–532. doi:10.1139/t94-061

Gaiser, T., U. Perkons, P.M. Küpper, T. Kautz, D. Uteau-Puschmann, F. Ewert, et al. 2013. Modeling biopore effects on root growth and biomass production on soils with pronounced sub-soil clay accumulation. Ecol. Modell. 256:6–15. doi:10.1016/j.ecolmodel.2013.02.016

Gao, W., C. Watts, T. Ren, and W. Whalley. 2012. The effects of compaction and soil drying on penetrometer resistance. Soil Tillage Res. 125:14–22. doi:10.1016/j.still.2012.07.006

German Weather Service. 2017. Climate Data Center: Daily soil temperature. [Database.] Deutscher Wetterdienst, Offenbach. ftp://ftp-cdc.dwd.de/pub/CDC/observations_germany/climate/daily/soil_temperature/ (accessed 13 Nov. 2017).

Golabi, M., D. Radcliffe, W. Hargrove, and E. Tollner. 1995. Macropore effects in conventional tillage and no-tillage soils. J. Soil Water Conserv. 50:205–210.

Good, S.P., D. Noone, and G. Bowen. 2015. Hydrologic connectivity constrains partitioning of global terrestrial water fluxes. Science 349:175–177. doi:10.1126/science.aaa5931

Grzesiak, M.T. 2009. Impact of soil compaction on root architecture, leaf water status, gas exchange and growth of maize and triticale seedlings. Plant Root 3:10–16. doi:10.3117/plantroot.3.10

Han, E., T. Kautz, U. Perkons, D. Uteau, S. Peth, N. Huang, et al. 2015. Root growth dynamics inside and outside of soil biopores as affected by crop sequence determined with the profile wall method. Biol. Fertil. Soils 51:847–856. doi:10.1007/s00374-015-1032-1

Hirth, J., B. McKenzie, and J. Tisdall. 2005. Ability of seedling roots of *Lolium perenne* L. to penetrate soil from artificial biopores is modified by soil bulk density, biopore angle and biopore relief. Plant Soil 272:327–336. doi:10.1007/s11104-004-5764-1

Holland, J.M. 2004. The environmental consequences of adopting conservation tillage in Europe: Reviewing the evidence. Agric. Ecosyst. Environ. 103:1–25. doi:10.1016/j.agee.2003.12.018

Jarvis, N., J. Koestel, and M. Larsbo. 2016. Understanding preferential flow in the vadose zone: Recent advances and future prospects. Vadose Zone J. 15(12). doi:10.2136/vzj2016.09.0075

Javaux, M., T. Schröder, J. Vanderborght, and H. Vereecken. 2008. Use of a three-dimensional detailed modeling approach for predicting root water uptake. Vadose Zone J. 7:1079–1088. doi:10.2136/vzj2007.0115

Kautz, T. 2015. Research on subsoil biopores and their functions in organically managed soils: A review. Renew. Agric. Food Syst. 30:318–327. doi:10.1017/S1742170513000549

Kautz, T., M. Luesebrink, S. Paetzold, D. Vetterlein, R. Pude, M. Athmann, et al. 2014. Contribution of anecic earthworms to biopore formation during cultivation of perennial ley crops. Pedobiologia 57:47–52. doi:10.1016/j.pedobi.2013.09.008

Kautz, T., U. Perkons, M. Athmann, R. Pude, and U. Köpke. 2013. Barley roots are not constrained to large-sized biopores in the subsoil of a deep Haplic Luvisol. Biol. Fertil. Soils 49:959–963. doi:10.1007/s00374-013-0783-9

Kautz, T., C. Stumm, R. Kösters, and U. Köpke. 2010. Effects of perennial fodder crops on soil structure in agricultural headlands. J. Plant Nutr. 173:490–501. doi:10.1002/jpln.200900216

Kirkegaard, J., J. Lilley, G. Howe, and J. Graham. 2007. Impact of subsoil water use on wheat yield. Aust. J. Agric. Res. 58:303–315. doi:10.1071/AR06285

Klosterhalfen, A., M. Herbst, L. Weihermüller, A. Graf, M. Schmidt, A. Stadler, et al. 2017. Multi-site calibration and validation of a net ecosystem carbon exchange model for croplands. Ecol. Modell. 363:137–156. doi:10.1016/j.ecolmodel.2017.07.028

Kobel-Lamparski, A., and F. Lamparski. 1987. Burrow constructions during the development of *Lumbricus badensis* individuals. Biol. Fertil. Soils 3:125–129.

Koevoets, I.T., J.H. Venema, J.T.M. Elzenga, and C. Testerink. 2016. Roots withstanding their environment: Exploiting root system architecture responses to abiotic stress to improve crop tolerance. Front. Plant Sci. 7:1335. doi:10.3389/fpls.2016.01335

Konôpka, B., L. Pages, and C. Doussan. 2009. Soil compaction modifies morphological characteristics of seminal maize roots. Plant Soil Environ. 55:1–10. doi:10.17221/380-PSE

Lancashire, P.D., H. Bleiholder, T.V.D. Boom, P. Langelüddeke, R. Stauss, E. Weber, and A. Witzenberger. 1991. A uniform decimal code for growth stages of crops and weeds. Ann. Appl. Biol. 119:561–601. doi:10.1111/j.1744-7348.1991.tb04895.x

Landl, M., K. Huber, A. Schnepf, J. Vanderborght, M. Javaux, A.G. Bengough, and H. Vereecken. 2017. A new model for root growth in soil with macropores. Plant Soil 415:99–116. doi:10.1007/s11104-016-3144-2

Loague, K., and R.E. Green. 1991. Statistical and graphical methods for evaluating solute transport models: Overview and application. J. Contam. Hydrol. 7:51–73. doi:10.1016/0169-7722(91)90038-3

Luo, L., H. Lin, and P. Halleck. 2008. Quantifying soil structure and preferential flow in intact soil using X-ray computed tomography. Soil Sci. Soc. Am. J. 72:1058–1069. doi:10.2136/sssaj2007.0179

McKenzie, B., A. Bengough, P. Hallett, W. Thomas, B. Forster, and J. McNicol. 2009. Deep rooting and drought screening of cereal crops: A novel field-based method and its application. Field Crops Res. 112:165–171. doi:10.1016/j.fcr.2009.02.012

Meunier, F., M. Javaux, V. Couvreur, X. Draye, and J. Vanderborght. 2016. A new model for optimizing the water acquisition of root hydraulic architectures over full crop cycles. In: IEEE International Conference on Functional-Structural Plant Growth Modeling, Simulation, Visualization and Applications (FSPMA), Qingdao, China. 7–11 Nov. 2016. IEEE, New York. doi:10.1109/FSPMA.2016.7818300

Meunier, F., M. Zarebanadkouki, M.A. Ahmed, A. Carminati, V. Couvreur, and M. Javaux. 2018. Hydraulic conductivity of soil-grown lupine and maize unbranched roots and maize root–-shoot junctions. J. Plant Physiol. doi:10.1016/j.jplph.2017.12.019

Mo, X., and S. Liu. 2001. Simulating evapotranspiration and photosynthesis of winter wheat over the growing season. Agric. For. Meteorol. 109:203–222. doi:10.1016/S0168-1923(01)00266-0

Mualem, Y. 1976. A new model for predicting the hydraulic conductivity of unsaturated porous media. Water Resour. Res. 12:513–522. doi:10.1029/WR012i003p00513

Nakamoto, T. 2000. The distribution of wheat and maize roots as influenced by biopores in a subsoil of the Kanto loam type. Plant Prod. Sci. 3:140–144. doi:10.1626/pps.3.140

Naveed, M., P. Moldrup, M.G. Schaap, M. Tuller, R. Kulkarni, H.-J. Vogel, and L.W. de Jonge. 2016. Prediction of biopore- and matrix-dominated flow from X-ray CT-derived macropore network characteristics. Hydrol. Earth Syst. Sci. 20:4017–4030. doi:10.5194/hess-20-4017-2016

Nielsen, M.H., M. Styczen, V. Ernstsen, C.T. Petersen, and S. Hansen. 2010. Field study of preferential flow pathways in and between drain trenches. Vadose Zone J. 9:1073–1079. doi:10.2136/vzj2010.0013.

Pagenkemper, S.K., M. Athmann, D. Uteau, T. Kautz, S. Peth, and R. Horn. 2015. The effect of earthworm activity on soil bioporosity: Investigated with X-ray computed tomography and endoscopy. Soil Tillage Res. 146:79–88. doi:10.1016/j.still.2014.05.007

Pagenkemper, S.K., S. Peth, D.U. Puschmann, and R. Horn. 2013. Effects of root-induced biopores on pore space architecture investigated with industrial X-ray computed tomography. In: S.H. Anderson and J.W. Hopmans, editors, Soil–water–root processes: Advances in tomography and imaging. SSSA Spec. Publ. 61. SSSA, Madison, WI. doi:10.2136/sssaspecpub61.c4

Passioura, J.B. 2002. Soil conditions and plant growth. Plant Cell Environ. 25:311–318. doi:10.1046/j.0016-8025.2001.00802.x

Perkons, U., T. Kautz, D. Uteau, S. Peth, V. Geier, K. Thomas, et al. 2014. Root-length densities of various annual crops following crops with contrasting root systems. Soil Tillage Res. 137:50–57. doi:10.1016/j.still.2013.11.005

Peth, S., R. Horn, F. Beckmann, T. Donath, J. Fischer, and A. Smucker. 2008. Three-dimensional quantification of intra-aggregate pore-space features using synchrotron-radiation-based microtomography. Soil Sci. Soc. Am. J. 72:897–907. doi:10.2136/sssaj2007.0130

Pitkänen, J., and V. Nuutinen. 1997. Distribution and abundance of burrows formed by *Lumbricus terrestris* L. and *Aporrectodea caliginosa* Sav. in the soil profile. Soil Biol. Biochem. 29:463–467. doi:10.1016/S0038-0717(96)00040-5

Porter, J.R., and M. Gawith. 1999. Temperatures and the growth and development of wheat: A review. Eur. J. Agron. 10:23–36. doi:10.1016/S1161-0301(98)00047-1

Richards, L. 1931. Capillary conduction of liquids through porous mediums. Physics 1:318–333. doi:10.1063/1.1745010

Ritchie, J.T. 1972. Model for predicting evaporation from a row crop with incomplete cover. Water Resour. Res. 8:1204–1213. doi:10.1029/WR008i005p01204

Rosquete, M.R., D. von Wangenheim, P. Marhavý, E. Barbez, E.H. Stelzer, E. Benková, et al. 2013. An auxin transport mechanism restricts positive orthogravitropism in lateral roots. Curr. Biol. 23:817–822. doi:10.1016/j.cub.2013.03.064

Sanderson, J., F.C. Whitbread, and D. Clarkson. 1988. Persistent xylem cross-walls reduce the axial hydraulic conductivity in the apical 20 cm of barley seminal root axes: Implications for the driving force for water movement. Plant Cell Environ. 11:247–256. doi:10.1111/j.1365-3040.1988.tb01143.x

Shipitalo, M.J., V. Nuutinen, and K.R. Butt. 2004. Interaction of earthworm burrows and cracks in a clayey, subsurface-drained, soil. Appl. Soil Ecol. 26:209–217. doi:10.1016/j.apsoil.2004.01.004

Šimůnek, J., M.Th. van Genuchten, and M. Šejna. 2016. Recent developments and applications of the HYDRUS computer software packages. Vadose Zone J. 15(7). doi:10.2136/vzj2016.04.0033

Somma, F., V. Clausnitzer, and J.W. Hopmans. 1998. An algorithm for three-dimensional, simultaneous modeling of root growth, transient soil water flow and solute transport and uptake. Version 2.1. Dep. of Land, Air and Water Resources Pap. 100034. Univ. of California, Davis.

Stirzaker, R., J. Passioura, and Y. Wilms. 1996. Soil structure and plant growth: Impact of bulk density and biopores. Plant Soil 185:151–162. doi:10.1007/BF02257571

Taylor, H.M., and L.F. Ratliff. 1969. Root elongation rates of cotton and peanuts as a function of soil strength and soil water content. Soil Sci. 108:113–119. doi:10.1097/00010694-196908000-00006

Tazawa, M., E. Ohkuma, M. Shibasaka, and S. Nakashima. 1997. Mercurial-sensitive water transport in barley roots. J. Plant Res. 110:435–442. doi:10.1007/BF02506803

Tóth, B., M. Weynants, A. Nemes, A. Makó, G. Bilas, and G. Tóth. 2015. New generation of hydraulic pedotransfer functions for Europe. Eur. J. Soil Sci. 66:226–238. doi:10.1111/ejss.12192

Tracy, S.R., C.R. Black, J.A. Roberts, and S.J. Mooney. 2011. Soil compaction: A review of past and present techniques for investigating effects on root growth. J. Sci. Food Agric. 91:1528–1537. doi:10.1002/jsfa.4424

Tracy, S.R., C.R. Black, J.A. Roberts, C. Sturrock, S. Mairhofer, J. Craigon, and S.J. Mooney. 2012. Quantifying the impact of soil compaction on root system architecture in tomato (*Solanum lycopersicum*) by X-ray micro-computed tomography. Ann. Bot. 110:511–519. doi:10.1093/aob/mcs031

Uteau, D., S.K. Pagenkemper, S. Peth, and R. Horn. 2013. Root and time dependent soil structure formation and its influence on gas transport in the subsoil. Soil Tillage Res. 132:69–76. doi:10.1016/j.still.2013.05.001

Valentine, T., P. Hallet, K. Binnie, M. Young, G. Squire, and G. Bengough. 2012. Soil strength and macropore volume limit root elongation rates in many UK agricultural soils. Ann. Bot. 110:259–270. doi:10.1093/aob/mcs118

van Genuchten, M.Th. 1980. A closed-form equation for predicting the hydraulic conductivity of unsaturated soils. Soil Sci. Soc. Am. J. 44:892–898. doi:10.2136/sssaj1980.03615995004400050002x

Veen, B.W., and F.R. Boone. 1990. The influence of mechanical resistance and soil water on the growth of seminal roots of maize. Soil Tillage Res. 16:219–226. doi:10.1016/0167-1987(90)90031-8

Vereecken, H., A. Schnepf, J.W. Hopmans, M. Javaux, D. Or, T. Roose, et al. 2016. Modeling soil processes: Review, key challenges, and new perspectives. Vadose Zone J. 15(5). doi:10.2136/vzj2015.09.0131

Wasson, A.P., R.A. Richards, R. Chatrath, S.C. Misra, S.V.S. Prasad, G.J. Rebetzke, et al. 2012. Traits and selection strategies to improve root systems and water uptake in water-limited wheat crops. J. Exp. Bot. 63:3485–3498. doi:10.1093/jxb/ers111

Watt, M., L.J. Magee, and M.E. McCully. 2008. Types, structure and potential for axial water flow in the deepest roots of field-grown cereals. New Phytol. 178:135–146. doi:10.1111/j.1469-8137.2007.02358.x

Whalley, W., J. To, B. Kay, and A. Whitmore. 2007. Prediction of the penetrometer resistance of soils with models with few parameters. Geoderma 137:370–377. doi:10.1016/j.geoderma.2006.08.029

White, R., and J. Kirkegaard. 2010. The distribution and abundance of wheat roots in a dense, structured subsoil: Implications for water uptake. Plant Cell Environ. 33:133–148. doi:10.1111/j.1365-3040.2009.02059.x

Wöhling, T., S. Gayler, E. Priesack, J. Ingwersen, H.-D. Wizemann, P. Högy, et al. 2013. Multiresponse, multiobjective calibration as a diagnostic tool to compare accuracy and structural limitations of five coupled soil–plant models and CLM3.5. Water Resour. Res. 49:8200–8221. doi:10.1002/2013WR014536

Young, I.M. 1998. Biophysical interactions at the root–soil interface: A review. J. Agric. Sci. 130:1–7. doi:10.1017/S002185969700498X